Uncovering the Tumor-Suppressive Roles of miR-940, miR-375, and miR-326 in Adrenocortical Carcinoma via ceRNA Network Analysis

Javad Omidi[1*]
[1]Department of Chemical Engineering, Columbia University, New York, NY 10027, USA
[*]Corresponding Author Email: jo2668@columbia.edu

Abstract

Adrenocortical carcinoma (ACC) is a rare endocrine malignancy with poor prognosis and limited therapeutic strategies. In this study, transcriptomic profiles from TCGA, GTEx 2025, and miRNATissueAtlas 2025 were integrated to construct ceRNA networks specific to tumor and normal adrenal tissues, leveraging a novel integrative analytical framework specifically developed in this study. Network topology revealed substantial rewiring in tumors, with miR-940 emerging as a tumor-exclusive hub, and miR-375 and miR-326 losing centrality despite marked downregulation. Experimentally validated and negatively correlated miRNA–mRNA interactions were identified, highlighting suppression of key oncogenes. Functional enrichment and PPI analyses demonstrated that the targets of these miRNAs are involved in pathways such as cell cycle regulation, EMT, and transcriptional activation. Survival analysis of target genes confirmed their prognostic relevance. Notably, miR-940 exhibited increased expression in radiation-treated patients, indicating therapy-responsive regulatory response, while miR-375 and miR-326 showed stable profiles. Cross-cancer expression analysis further supported the tumor-suppressive roles of all three miRNAs across multiple malignancies. These findings collectively establish miR-940, miR-375, and miR-326 as context-dependent tumor suppressors in ACC with potential therapeutic and biomarker utility.

Keywords: Adrenocortical Carcinoma (ACC), Tumor Suppressor microRNAs, ceRNA Network, Transcriptomic Analysis

1. Introduction

Adrenocortical carcinoma (ACC) has been recognised as a rare yet aggressive malignancy of the adrenal cortex, occurring in only 0.7–2 cases per million people annually [1]. A bimodal age distribution has been described, chiefly involving children < 5 years and adults 40–60 years [2]. Although surgical resection has been employed as first-line therapy, 5-year survival of merely 16–47 % has been reported because of frequent recurrence and metastasis [3]. Tumourigenesis has been linked to dysregulated Wnt/β-catenin signalling, IGF2 over-expression and germ-line TP53 mutations, especially in Li-Fraumeni syndrome [4 and 5], and drug-development progress has been hampered by the disease's rarity (The Cancer Genome Atlas Research Network, 2016).

Non-coding RNAs (ncRNAs)—miRNAs, lncRNAs and circRNAs—have been identified as critical regulators of transcriptional, post-transcriptional and epigenetic programmes in cancer [6]. Their interactions have been framed by the competing endogenous RNA (ceRNA) hypothesis, under which transcripts sharing microRNA-response elements (MREs) are believed to modulate one another by competing for miRNA binding [7]. Canonical ceRNA activity has been demonstrated for lncRNA HOTAIR and circRNA CDR1as in breast and colorectal tumours, respectively [8 and 9], and ceRNA-network dysregulation has been implicated in glioblastoma, hepatocellular and lung cancers, correlating with poor prognosis [10].

Within ceRNA networks, certain miRNAs have been reported as topological hubs that orchestrate extensive gene-expression programmes [11]. By simultaneously interacting with numerous lncRNAs, circRNAs and mRNAs through shared MREs, these hubs have been shown to modulate oncogenes and tumour suppressors across multiple pathways [12]. MiR-21 and miR-155 have consistently been identified as high-degree nodes in breast, lung and colorectal malignancies, underscoring broad roles in apoptosis, immunity and proliferation [13]. Large-scale comparisons have revealed extensive miRNA-mediated network rewiring between normal and malignant tissues, highlighting hub targeting as a potential therapeutic lever [14–16], and pan-cancer surveys have indicated that lncRNAs such as LINC01929 act as master regulators of metastasis [14].

In ACC, prognostic relevance has been assigned to miR-195 and miR-483-5p, whose dysregulated expression has been correlated with adverse clinical outcomes [17]. Genome-wide profiling has also shown pronounced down-regulation of miR-139 and other tumour-suppressive miRNAs relative to benign adenomas, implying growth-restraining functions [18]. A multi-omics analysis by TCGA has delineated an aggressive C1A subtype characterised by elevated miR-483-5p and reduced miR-195/497 expression, reaffirming the value of miRNA signatures in tumour stratification [5].

The tumour-suppressive roles of miR-940, miR-375 and miR-326 have been documented across diverse malignancies. MiR-940 down-regulation has been reported in hepatocellular carcinoma, where over-expression has inhibited proliferation and invasion by targeting CXCR2 and has been associated with improved survival [19]. Similar tumour-suppressive effects have been observed in

oesophageal squamous cell carcinoma [20] and triple-negative breast cancer through ZNF24 repression [21]. MiR-375 has been characterised as a potent suppressor of epithelial–mesenchymal transition, proliferation and drug resistance in multiple cancers [22]; its targeting of RON in gastric cancer has inhibited growth and invasion [23], and CIP2A repression in oral cancer has curtailed tumour aggressiveness [24]. Even when up-regulated in prostate cancer, miR-375 has been shown to attenuate metastatic potential by silencing oncogenic ceRNA hubs [25]. MiR-326 down-regulation has been linked to enhanced tumour growth; its forced expression has suppressed cervical-cancer proliferation via ELK1 inhibition [26], reduced triple-negative breast-cancer metastasis via SOX12 repression [27] and limited colorectal-cancer progression by targeting NOB1 [28]. Despite these extensive data, the contributions of miR-940, miR-375 and miR-326 to ACC biology have yet to be elucidated.

Accordingly, a first-of-its-kind, comprehensive systems-level analysis was conducted to evaluate the tumor-suppressive potential of miR-940, miR-375, and miR-326 within the ceRNA network of adrenocortical carcinoma (ACC). For the first time, these miRNAs are identified and functionally characterized as key regulatory components in ACC, using integrated large-scale transcriptomic datasets from TCGA [29] as well as newly released GTEx 2025 [30] and miRNATissueAtlas 2025 [31], in combination with experimentally validated miRNA–mRNA interactions and advanced network-based topological methods. While their tumor-suppressive roles have been established in other malignancies, their discovery and systematic analysis in the context of ACC is entirely novel. This framework enabled the elucidation of their regulatory centrality, context-specific expression patterns, and mechanistic impact in ACC, providing new and unprecedented insights into their potential as diagnostic and prognostic biomarkers and their involvement in the molecular pathogenesis of this rare adrenal tumor.

2. Materials and Methods

2.1 Data Acquisition and Preprocessing

Transcriptomic data for Adrenocortical Carcinoma (ACC) were retrieved from The Cancer Genome Atlas (TCGA) [22] and Genotype-Tissue Expression (GTEx 2025) [28] databases to ensure comprehensive representation of tumor and normal adrenal tissues. Specifically, RNA-Seq and miRNA-Seq datasets from 78 ACC tumor samples were downloaded from TCGA-ACC, encompassing both gene and microRNA expression profiles. All tumor data were collated and merged across samples to generate structured expression matrices for downstream analysis.

To represent the normal tissue counterpart, RNA-Seq and miRNA-Seq data from 250 adrenal gland samples were obtained from GTEx 2025 [28]. For miRNA data, additional filtering was required to remove redundant entries and retain only mature human miRNAs. The miRNA data has been reported recently in GTEx 2025 Preprocessing steps included data harmonization, format standardization, and the generation of unified case-by-feature matrices for both RNA and miRNA datasets. A summary of the datasets, sample types, and processing steps is provided in Table 1.

Given the limited availability and recent inclusion of miRNA expression data in GTEx 2025 [30], especially for adrenal gland tissues, a complementary dataset was utilized to enhance the analysis of hsa-miR-466. Specifically, normalized miRNA expression profiles from the miRNATissueAtlas 2025 [31] were incorporated, which includes harmonized RPMM-based data from 630 normal adrenal gland samples. This dataset provided broader coverage and improved statistical power for downstream correlation and network analyses.

Table 1. Summary of transcriptomic datasets used in this study, including RNA-Seq and miRNA-Seq data from TCGA [29], GTEx 2025 [30], miRNATissueAtlas 2025 [31] and for ACC tumor and normal adrenal tissues.

Source	Dataset Name	Sample Type	Number of Samples	Data Type	Platform	Normalization	Notes
TCGA [29]	TCGA-ACC	Tumor	78	RNA-Seq (Gene Expression)	Illumina HiSeq	FPKM / TPM	Includes matched clinical metadata
GTEx 2025 [30]	Adrenal Gland	Normal	250	RNA-Seq (Gene Expression)	Illumina HiSeq	TPM	Healthy controls, not cancer-specific
TCGA [29]	TCGA-ACC	Tumor	78	miRNA-Seq	Illumina HiSeq	RPM (Reads per Million)	Mature miRNA expression
GTEx 2025 [30]	Adrenal Gland	Normal	250	miRNA-Seq	Illumina HiSeq	Read count / TPM	Mature hsa-miRNAs retained after preprocessing
miRNA Tissue Atlas 2025 [31]	Adrenal Gland	Normal	630	miRNA-Seq	Illumina small RNA-Seq	RPMM (Reads per million mapped)	Harmonized .h5ad; only mature hsa-miRNAs retained

2.2 Quality Control and Filtering Strategies

Quality control and expression filtering were applied uniformly across mRNA and miRNA datasets to improve data reliability while preserving relevant biological signals. To eliminate transcriptionally inactive or near-zero expression genes, a filtering step was applied whereby genes with TPM (for RNA-Seq) or RPM (for miRNA) values less than 1 in more than 80% of the samples were excluded. This threshold was intentionally set at a permissive level to retain weakly expressed yet potentially informative transcripts, given the relatively small sample size in the ACC dataset. The aim was to minimize background noise while preserving subtle expression patterns that might otherwise be lost under stricter filtering criteria. Gene expression distributions were assessed visually after log-transformation to ensure consistency between tumor and normal samples and to

verify the effectiveness of the normalization process. No major deviations or technical artifacts were observed that warranted further sample removal. Although principal component analysis (PCA) and unsupervised clustering were considered for outlier detection, no samples showed patterns indicative of being technical outliers. Filtering steps were implemented using custom R scripts with consistent thresholds across mRNA and miRNA data. This filtering approach ensured the retention of biologically informative features while reducing technical noise, providing a solid foundation for subsequent integrative and network-based analyses.

2.3 Differential Expression Analysis

Differential expression analysis between normal and tumor adrenal tissue samples was conducted using the limma-voom pipeline [29] in R, which combines linear modeling with empirical Bayes moderation after precision weighting of log-transformed expression values through the voom method. This approach has been widely adopted for RNA-Seq transcriptomic data analysis. Raw RNA-Seq count data for both normal (GTEx 2025 [28]) and tumor (TCGA-ACC [22]) samples were first curated to retain only valid gene entries and to remove transcript version numbers. The two datasets were then merged by gene ID, and the unstranded count values were extracted to construct a unified count matrix representing all samples. To reduce noise and improve model stability, genes with low expression were filtered out prior to transformation. To account for library size differences and prepare the data for linear modeling, the filtered count matrix was transformed into log2-counts per million (log-CPM) using the voom function, which also estimated the mean–variance trend and assigned precision weights.

A design matrix was then constructed to define the two experimental groups—normal and tumor—with the normal group set as the reference level. Linear modeling was performed with lmFit, followed by empirical Bayes shrinkage via the eBayes function to improve variance estimation. Differentially expressed genes (DEGs) were extracted using the topTable function, ranking results by adjusted p-values using the Benjamini-Hochberg FDR correction. DEGs were selected based on an adjusted p-value < 0.05 and an absolute $|\log2 \text{ fold change}| > 1$. Final results were saved with corrected gene identifiers for downstream analyses. In total, 15,745 DEGs were identified, including 10,254 upregulated and 5,491 downregulated genes in tumor samples compared to normal.

2.4 Integration of miRNA-mRNA Interactions and ceRNA Network Construction

A comprehensive ceRNA network was constructed using transcriptomic data from 78 adrenocortical carcinoma (ACC) tumor samples obtained from The Cancer Genome Atlas (TCGA) [22] and 250 normal adrenal tissue samples from the Genotype-Tissue Expression (GTEx 2025) project [28]. After standardized preprocessing, miRNA and mRNA expression matrices were independently generated for tumor and normal conditions. Experimentally validated miRNA–mRNA interactions were retrieved using the multiMiR R package [30], which consolidates high-confidence interactions from databases such as miRTarBase, TarBase, and miRecords. Only

interactions classified under the "validated" category were retained to ensure biological credibility. To ensure that these experimentally supported interactions were functionally relevant in the context of ACC, each miRNA–mRNA pair was further evaluated using expression data specific to tumor and normal tissues. Pearson correlation coefficients were computed separately for tumor and normal samples to assess whether each pair exhibited a statistically significant inverse expression pattern. Interactions were retained only if they showed a negative correlation ($r < -0.3$, $p < 0.05$) in the corresponding condition. This two-step filtering approach—first based on experimental validation, then refined by disease-specific expression consistency—ensures that the resulting network accurately reflects regulatory dynamics in ACC. It should be noted that the constructed ceRNA network in this study focused exclusively on miRNA–mRNA interactions, without incorporating direct mRNA–mRNA crosstalk. Such a model is widely accepted in the field, as many recent studies have demonstrated that miRNA-mediated regulatory axes capture the essential topology and biological relevance of ceRNA networks even in the absence of explicit mRNA–mRNA edges.

2.5 Computational Tools and Programming Languages

All differential expression analyses (DEG) and correlation-based construction of the ceRNA regulatory network were performed using R (version 4.5.1). The limma package was applied for linear modeling and empirical Bayes moderation, following voom transformation of raw count data to stabilize the mean–variance relationship. In the preprocessing stage, the edgeR package was used for filtering lowly expressed genes and for preliminary normalization where necessary. Correlation analyses between miRNA and mRNA expression profiles were conducted using the psych and Hmisc packages to compute Pearson and Spearman coefficients. To construct a biologically meaningful miRNA–mRNA interaction network, the multiMiR package was employed to retrieve experimentally validated and predicted interactions from multiple databases, including miRTarBase, TargetScan, and miRDB. Additional data wrangling and visualization within R were carried out using functions from the tidyverse ecosystem, particularly ggplot2, for exploratory plots.

For network visualization and high-resolution figure generation, Python (version 3.13.5) was employed. Expression data matrices and interaction results were first structured and processed using pandas and numpy. Correlation heatmaps, volcano plots, and other expression-based visualizations were generated using matplotlib and seaborn. Graph-based visualizations of the miRNA–mRNA regulatory network were created with networkx, allowing for computation of topological metrics such as betweenness centrality and layout optimization. Where necessary, dimensionality reduction and clustering visualization were facilitated by scikit-learn. In specific instances involving machine learning–based prediction and model interpretation, shap and lime were optionally utilized to illustrate feature importance and interaction effects. All computational analyses were performed on a local workstation, and scripts were developed in a modular and reproducible manner.

3. Results and Discussion

3.1 Construction of the ceRNA Network in ACC

Analysis of the ceRNA networks constructed from normal and tumor transcriptomes of ACC, reveals substantial differences in regulatory architecture between physiological and cancerous states. In the normal adrenal network, hsa-miR-375 and hsa-miR-326 were among the top six hub nodes. These miRNAs exhibit discrete, modular connectivity patterns, suggesting that post-transcriptional regulation in normal tissue is compartmentalized and functionally localized. In contrast, the tumor-specific network demonstrates a markedly more interconnected and compact topology, indicative of extensive regulatory rewiring in ACC. Within this network, the dominant hubs include hsa-miR-940 which is not central or even active in the normal network. The emergence of these tumor-exclusive hubs reflects a significant shift in the balance and influence of miRNA-driven regulation under oncogenic pressure.

These observations are further substantiated by the quantitative analysis, which compares betweenness centrality values of the most influential miRNAs across normal and tumor networks. In the comparative analysis of the ceRNA networks, substantial shifts in hub miRNAs are observed between normal and tumor conditions. In the tumor network, miR-940 exhibits the highest betweenness centrality, reflecting a pronounced reorganization of regulatory control toward tumor-specific modules. Conversely, in the normal network, miR-326 and miR-375 serve as the principal hubs, while both display reduced or negligible centrality in the tumor context. These reciprocal changes highlight the dynamic rewiring of miRNA-mediated interactions in ACC and reveal context-specific hub miRNAs with potential utility in biomarker discovery and therapeutic targeting.

The constructed ceRNA network consisted of over 72 nodes and 57 edges in normal tissues and expanded to more than 267 nodes and 210 edges in tumor samples, indicating substantial topological complexity in the malignant state. In GTEx 2025-derived normal samples [30], several hub miRNAs identified in tumor tissues were not detected. This absence, however, is likely attributable to the stringent preprocessing pipeline and database-specific filtering applied in GTEx 2025 [30], rather than a true lack of biological expression. Supporting this, data from the miRNATissueAtlas 2025 [31] confirm that many of these miRNAs are indeed expressed in normal adrenal tissues, underscoring the importance of integrating complementary datasets to obtain a more comprehensive view of miRNA expression.

Building upon the comparative analysis of expression patterns and network centrality among hub miRNAs in normal and tumor ceRNA networks, three candidates—miR-940, miR-375, and miR-326—emerged as potential tumor suppressors warranting further investigation. Notably, miR-940 appears as a dominant hub exclusively in the tumor-specific network, despite exhibiting relatively low expression levels, suggesting a structurally central yet potentially inhibitory regulatory role in the malignant state. Conversely, miR-375 and miR-326, which occupy prominent central positions

in the normal network, show markedly reduced centrality in the tumor context. This downshifting may reflect oncogenic suppression of their physiological regulatory functions. Collectively, these findings highlight the context-dependent regulatory roles of these miRNAs and support their candidacy as tumor suppressors in ACC, meriting comprehensive functional validation in future studies.

3.2 Expression Profile and Tumor Stage Association of Central miRNAs

Figure 1a presents the expression profiles of three candidate tumor-suppressive miRNAs—miR-940, miR-375, and miR-326—in normal versus tumor adrenal tissues. In all three cases, a marked downregulation is observed in tumor samples, as measured by $\log_2(RPM + 0.01)$, with statistically distinct distribution patterns. For the comparisons shown in Figure 1, p-values were calculated using the limma package, which applies a linear modeling framework combined with an empirical Bayes moderated t-test for differential expression analysis. Statistical significance is represented by asterisks: *** $p < 0.001$; ** $p < 0.01$; * $p < 0.05$; ns not significant. Notably, miR-375 exhibits the highest expression in normal tissue, followed by a significant decline in tumors, suggesting loss of a strong regulatory influence. Similarly, miR-326 and miR-940 display consistent downregulation in tumors, despite their emergence as structurally central nodes in the tumor-specific ceRNA network. These inverse relationships between expression level and network centrality reinforce their potential roles as tumor suppressors in ACC and underscore the importance of further mechanistic validation.

The expression landscape of miR-940, miR-375, and miR-326 is further clarified through violin plot analysis, revealing consistent and statistically significant downregulation in tumor tissues relative to normal counterparts (***, $P < 0.001$). The distinct narrowing and leftward shift in distribution observed for each miRNA in the tumor group suggests both suppression of expression and reduced heterogeneity under malignant conditions. These expression patterns, coupled with their network centrality dynamics, strengthen the case for their functional roles as tumor-suppressive regulators in the context of ACC.

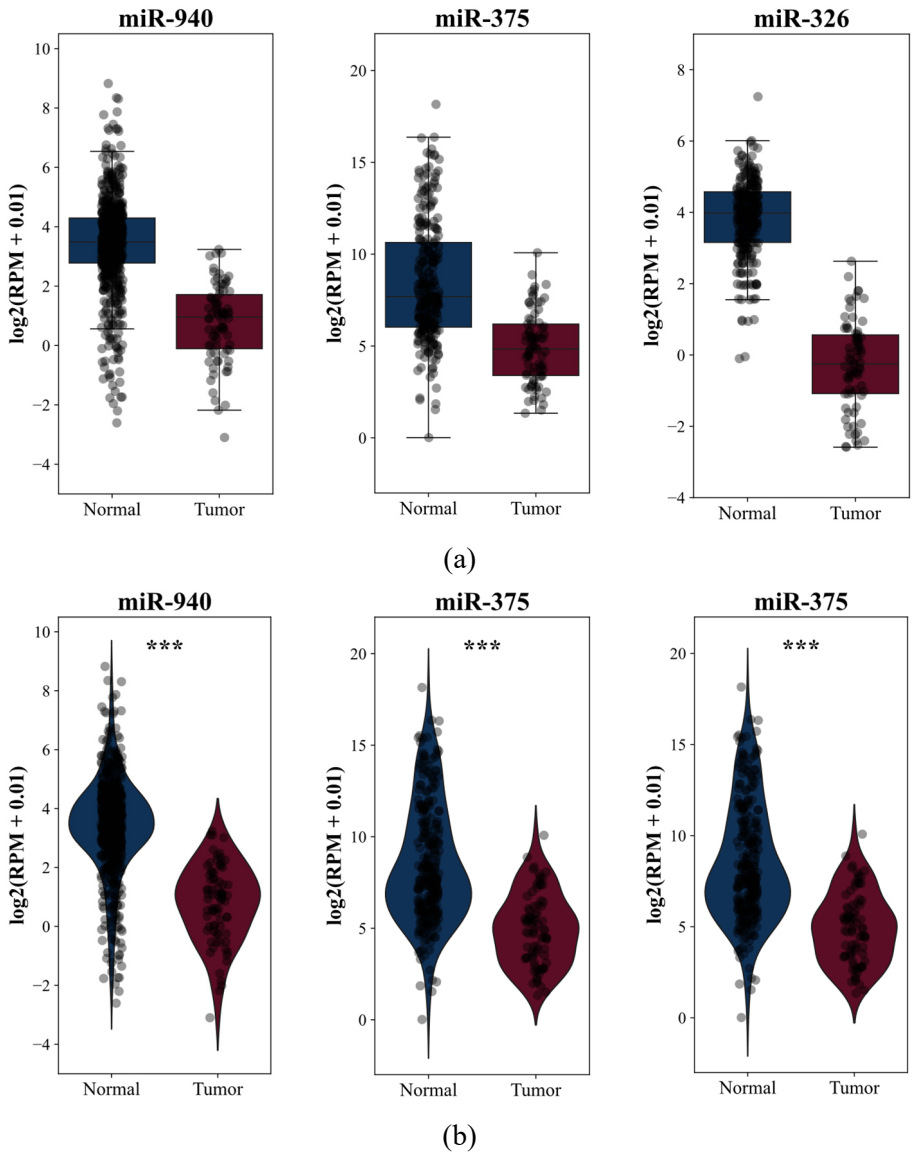

Figure 1. Box plots and violin plots of central miRNAs expression in Normal vs. Tumor tissue samples. These miRNAs exhibit statistically significant expression differences and are considered central regulators in the dataset. (Tumor: ACC TCGA [29], Normal: miR-940: miRNATissueAtlas 2025 [31], Normal: miR-375: GTEx 2025 [30], Normal: miR-375: GTEx 2025 [30])

3.3 Target Prediction of Central miRNAs

Experimentally validated and computationally predicted mRNA targets of miR-940, miR-375, and miR-326 were systematically compiled from miRTarBase [34] and miRDB databases [35]. All human targets (hsa) from miRTarBase were included regardless of the validation method, encompassing luciferase reporter assays, qRT-PCR, and Western blotting. In cases where the number of validated targets exceeded 200, prioritization was performed based on the number of supporting experimental records, and the top 200 genes were retained. For miR-940, supporting evidence ranged from 6 to 35 entries in miRTarBase [34], while miRDB [35] predictions were

filtered using a score threshold > 80. Target sets for miR-375 and miR-326 were filtered with thresholds of 2–43 and 3–38 experimental records, and miRDB score cutoffs > 55 and > 75, respectively. This integrated approach allowed the selection of robust candidate targets combining empirical evidence and predictive confidence.

Subsequent correlation analysis was carried out using transcriptomic profiles from TCGA-ACC [29] to assess the regulatory relevance of the selected miRNA–mRNA pairs in the ACC context. Pearson correlation coefficients were calculated for each pair, and only interactions showing statistically significant inverse correlations ($r < -0.3$, $p < 0.05$) were retained. The resulting high-confidence target genes, presented in Table 2, represent a context-specific subset with putative functional relevance. A considerable proportion of these genes have been previously characterized as oncogenic drivers in other cancer types, further supporting the role of miR-940, miR-375, and miR-326 as potential tumor suppressors in adrenocortical carcinoma.

Table 2. Top predicted or experimentally validated target genes for central miRNAs. Target genes were selected based on prediction scores from miRDB [35] or experimental evidence from miRTarBase [34] validated by TCGA ACC dataset with tumor $r < -0.3$ and $p < 0.05$ and ENCORI (StarBase) database [36]).

Central miRNA	Top Target Genes	Evidence	Supporting Record Number Range	Dataset	Validation Source
miR-940	OGFRL1, IRAK3, CYP4V2, MPP7, CLCN5, PIK3C2B, CNOT4, ZBTB7A, SIGLEC8, PLEKHA2, THNSL1, PNPO, GNG7, GM2A, GK5	Experimental (HITS-CLIP, PAR-CLIP, CLIP-seq, HITS-CLIP | PAR-CLIP)	6 < & < 35	miRTarBase [34]	ACC TCGA Dataset & ENCORI (StarBase) [36]
miR-375	COL4A4, FGF7, ITPKB, ARID5B, SOX12, RBM39, MATR3, PHF6, RBM12B, DRAM1, PRDM1, XAF1, JUND, PHACTR2, PHC3, FBXO32, MSL2, EXOC6	Experimental (HITS-CLIP, PAR-CLIP, CLIP-seq, HITS-CLIP | PAR-CLIP)	2 < & < 43	miRTarBase [34]	ACC TCGA Dataset & ENCORI (StarBase) [36]
miR-326	ELFN2, HOOK3, XKR9, CPA4, KLHDC10, ZNF772, ATXN7L3B, ELMO2, GGA2, TMBIM4, SETD1B, ZNF814, GLYR1, TOM1L2, USH1G, MAVS,	Experimental (HITS-CLIP, PAR-CLIP, CLIP-seq, HITS-CLIP | PAR-CLIP)	3 < & < 38	miRTarBase [34]	ACC TCGA Dataset & ENCORI (StarBase) [36]

	CBX5, SLC27A1, DPF2				
miR-940	ZC4H2, PCCB, NFASC, HS3ST3B1, PRKN, FAM104B, PARD3B, FHIT, CKMT2	In Silico (AI)	Target Score > 80	miRDB [35]	ACC TCGA Dataset & ENCORI (StarBase) [36]
miR-375	ITPKB, CLEC5A, NR5A2, DNALI1, MBNL1, COLCA2, CPNE8, SGK3, MXI1, NOX4, PIGL, BAHCC1, SAMD8, TSPAN2, MGAT4A	In Silico (AI)	Target Score > 55	miRDB [35]	ACC TCGA Dataset & ENCORI (StarBase) [36]
miR-326	VLDLR, EPHX2, NPAS3, NLK, FBXO21, ZNF197, CFAP70, TK2, DNM1L, JADE1, RNF150, SOBP, PNISR, RALGAPA1, CDK15	In Silico (AI)	Target Score > 75	miRDB [35]	ACC TCGA Dataset & ENCORI (StarBase) [36]

Given that oncogenes are typically overexpressed in cancer and exhibit a $\log_2$ fold change (logFC) > 1, this section aimed to evaluate the extent to which miR-940, miR-375, and miR-326 target upregulated genes in ACC. An initial differential expression analysis was performed using the limma package, and the resulting data were visualized through a volcano plot (Figure 2). This analysis identified 2,465 genes in the upregulated region of the plot, representing potential oncogenic candidates in ACC. Pearson correlation analysis was subsequently applied between each miRNA and this subset of genes, with interactions filtered at a significance threshold of $r < -0.2$ and $p < 0.05$ to capture plausible inhibitory relationships. The results revealed that miR-940 negatively correlated with 122 upregulated genes, miR-375 with 31, and miR-326 with 81, indicating varying degrees of suppressive targeting among these miRNAs. These findings are presented in Figure 2 and summarized in Table 3, where the top 10 most significantly correlated genes for each miRNA are also listed. The volcano plot in Figure 2 further highlights the subset of upregulated genes targeted by each miRNA, providing a visual representation of their potential roles in modulating oncogene expression in ACC. The expression profiles and differential expression magnitudes of the top candidate genes from Table 4 are illustrated in Figure 3, which includes boxplots across tumor and normal tissues as well as $\log_2$ fold change values, providing additional support for their functional relevance in ACC.

Interestingly, the analysis revealed that the gene INSYN2B is concurrently targeted by all three central miRNAs—miR-940, miR-375, and miR-326—suggesting a shared regulatory mechanism

and potential functional importance in ACC. In addition, BLVRB and PLD4 were found to be jointly targeted by miR-940 and miR-375, while ACADL and ABHD11-AS1 were co-targeted by miR-940 and miR-326. The convergence of multiple tumor-suppressive miRNAs on these genes underscores their likely involvement in key oncogenic pathways and highlights them as promising candidates for future functional studies aimed at elucidating the molecular mechanisms underlying ACC progression.

Table 3. Summary of significantly correlated upregulated target genes for miR-940, miR-375, and miR-326 among 2,465 genes identified through differential expression analysis in TCGA ACC [29]. Correlation thresholds were set at $r < -0.2$ and $p < 0.05$. The top 10 genes per miRNA are shown with their respective logFC and p-value ranges.

Central miRNA	Regulation Type	% of Targeted Genes	r Range	p-value Range	Top 10 Selected Target Genes	logFC Range	p-value Range
miR-940	Up (2465 total)	4.95% (no 122)	< -0.2	< 0.05	BCL2L1, JAK3, GDF15, RASGRP1, IQGAP2, GRPR, ANGPTL6, CD82, CLGN, CLCN4	1.0007 6.4017	1.11e-157 0.0017
miR-375	Up (2465 total)	1.26% (no 31)	< -0.2	< 0.05	HSPB1, IL3RA, TNFRSF4, PLD4, LOXHD1, HSPB1P1, HSPB1P2, SEPTIN1, CDKL2, SNRPB	1.0007 6.4017	1.11e-157 0.0017
miR-326	Up (2465 total)	3.41% (no 84)	< -0.2	< 0.05	TWIST1, BMP4, DLK1, BSG, PRKACA, ILVBL, GPR143, CLCN4, SUB1P1, PLA2G4D	1.0007 6.4017	1.11e-157 0.0017

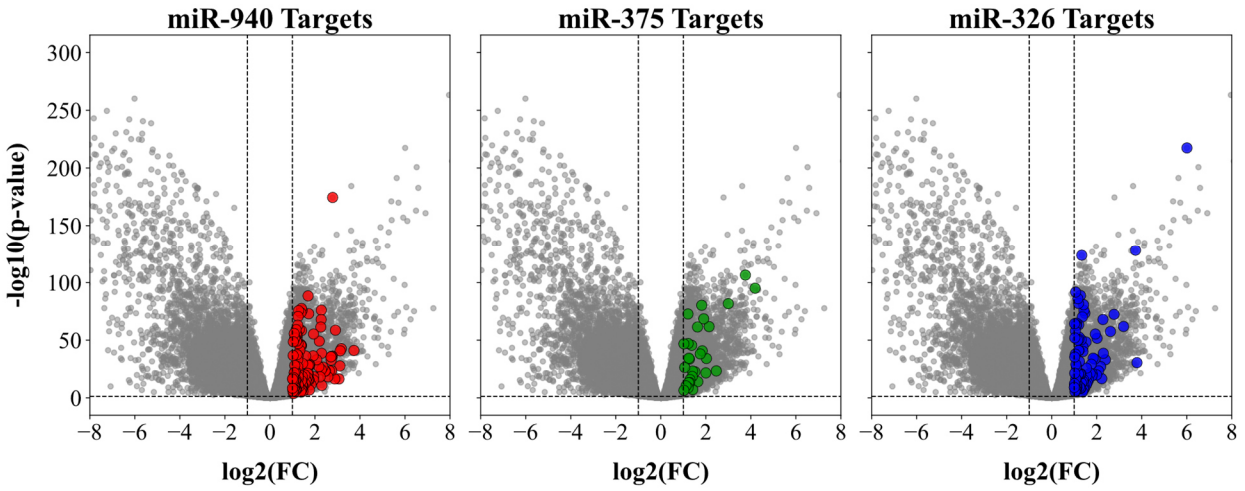

Figure 2. Volcano plot illustrating the upregulated genes in ACC ($logFC > 1$, $p < 0.05$). Target genes significantly correlated ($r < -0.2$, $p < 0.05$) with miR-940, miR-375, and miR-326 are highlighted.

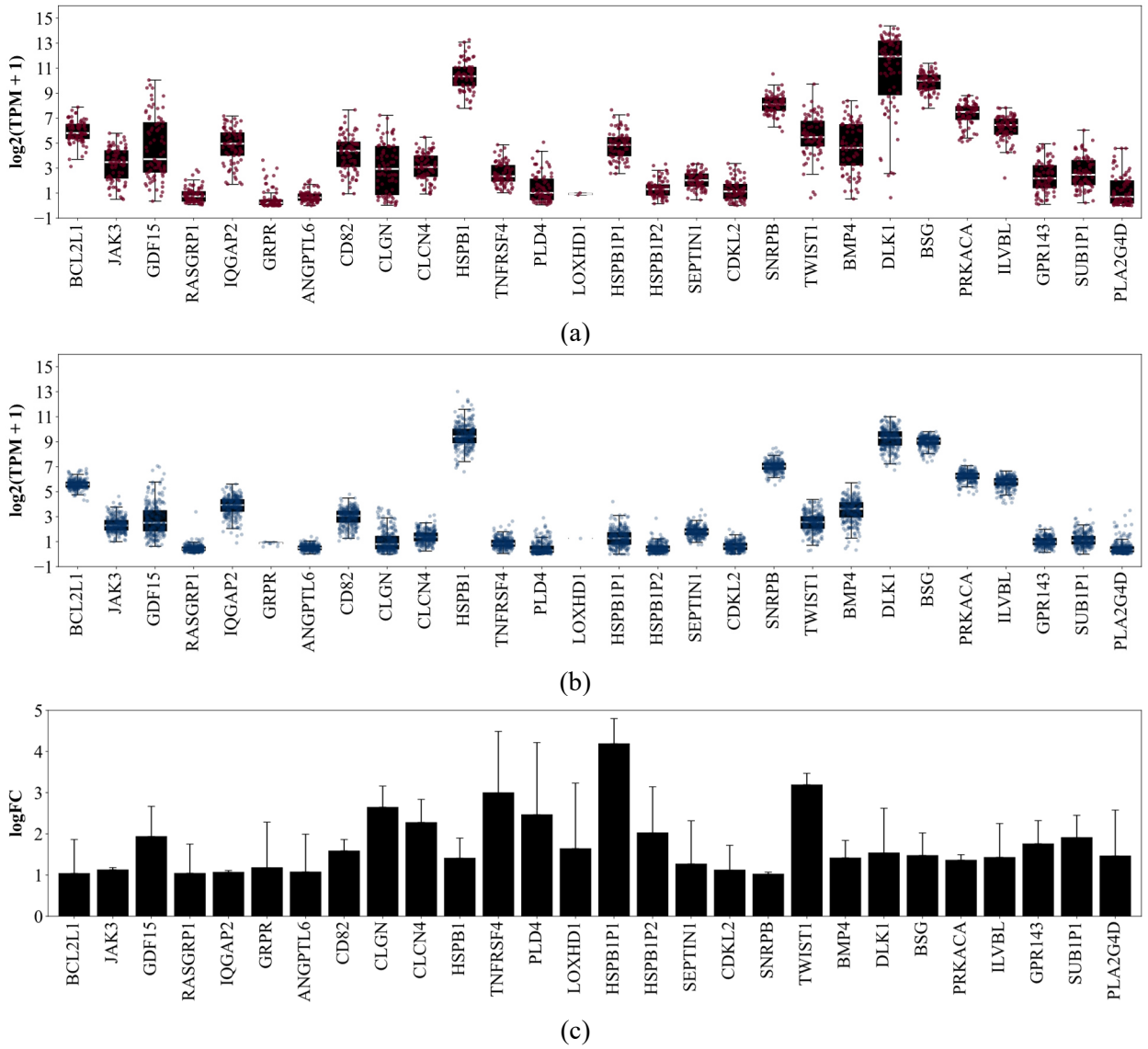

Figure 3. Expression analysis of representative target genes of miR-507 and miR-665 in ACC. (a–b) Boxplots showing expression levels across TCGA-ACC tumor samples [29] and GTEx 2025 normal adrenal tissues [30]; (c) log2 fold changes highlighting differential expression direction and magnitude. Targets include mitotic regulators, apoptotic mediators, and transcriptional modulators.

3.4 Target Prediction of Central miRNAs with Changing the Regulatory

To identify context-dependent regulatory shifts, a focused analysis was performed on miR-375 and miR-326 target upregulated genes that exhibited substantial changes in correlation patterns between normal and tumor conditions. Differential correlation analysis was based on Pearson's correlation coefficients (r) and associated p-values, using TCGA-ACC data [29] for tumor samples and GTEx 2025 normal adrenal tissues [30] for the normal state. miRNAs were correlated with their predicted or validated mRNA targets, and pairs showing significant changes in correlation ($p < 0.05$ in both conditions) were retained. Two major criteria were applied for prioritization: (1)

targets with a large absolute Δr (difference in correlation) between tumor and normal, and (2) targets that demonstrated a directional switch, specifically changing from a positive correlation in normal to a negative correlation in tumor, suggestive of a gain of post-transcriptional repression. This analysis was not extended to miR-940 due to unavailability of corresponding mrna seq profiles in miRNATissueAtlas 2025 [31] and absence of this miRNA in the GTEx 2025 miRNA dataset [30]. A curated list of representative target genes that met these criteria is summarized in Table 4.

The results revealed a subset of genes for which miRNA–mRNA correlations shifted dramatically between physiological and malignant contexts, implying dynamic regulatory rewiring. Notably, several targets of miR-375, including PLD4, TMCC3, and LOXHD1, exhibited strong positive correlations in normal tissue that became significantly negative in tumor samples, with Δr values exceeding 0.4. Similarly, miR-326 showed pronounced regulatory changes with targets such as LRRC3-DT, ZNF404, and C19orf48. These findings are illustrated in Figure 4, which depicts scatter plots of selected gene–miRNA pairs that exemplify either a reversal of correlation direction or a marked increase in negative regulatory strength. Together, these results support the notion that miR-375 and miR-326 engage in tumor-specific regulatory interactions that are not evident under normal physiological conditions, reinforcing their role as context-dependent repressors in ACC.

Table 4. List of target genes that exhibit a substantial shift in miRNA–mRNA correlation between normal and tumor samples.

Central miRNA	Target Genes	r (Normal)	p-value (Normal)	r (Tumor)	p-value (Tumor)	Δr	Direction Change	Evidence Source
miR-375	NAPSB	0.25235	0.000029	-0.32142	0.00387	0.57377	TRUE	TCGA Data Analysis
	PLD4	0.27415	0.000005	-0.25784	0.02178	0.53199	TRUE	
	TMCC3	0.25906	0.000017	-0.23123	0.04033	0.49029	TRUE	
	SEPTIN1	0.23801	0.000083	-0.25012	0.02621	0.48813	TRUE	
	LOXHD1	0.15468	0.011222	-0.32384	0.01024	0.47852	TRUE	
	SNX32	0.19189	0.001600	-0.24108	0.03349	0.43296	TRUE	
	TNFRSF4	0.14763	0.015570	-0.26109	0.02012	0.40873	TRUE	
	INSYN2B	-0.12235	0.045373	-0.27500	0.01854	0.15264	FALSE	
	HSPB1	-0.12259	0.044948	-0.26777	0.01704	0.14518	FALSE	
	BLVRB	-0.18249	0.002711	-0.22176	0.04952	0.03927	FALSE	
miR-326	LRRC3-DT	0.17822	0.003418	-0.25101	0.03895	0.42923	TRUE	
	ZNF404	0.13529	0.026786	-0.25215	0.03139	0.38744	TRUE	
	C19orf48	0.12080	0.048210	-0.23134	0.04892	0.35214	TRUE	
	SMIM10L2A	-0.15496	1.11e-02	-0.35142	0.00230	0.19645	FALSE	
	FRG1JP	-0.13338	2.90e-02	-0.32505	0.00501	0.19168	FALSE	
	HYDIN	-0.12601	3.93e-02	-0.28251	0.03663	0.15650	FALSE	
	CCDC96	-0.13248	3.01e-02	-0.28883	0.01320	0.15635	FALSE	
	IQGAP2	-0.23891	7.81e-05	-0.38318	0.00082	0.14427	FALSE	
	ATXN7L3B	-0.38891	4.15e-11	-0.24626	0.03571	0.14264	FALSE	
	ZNF768	-0.17929	3.23e-03	-0.31159	0.00729	0.13230	FALSE	

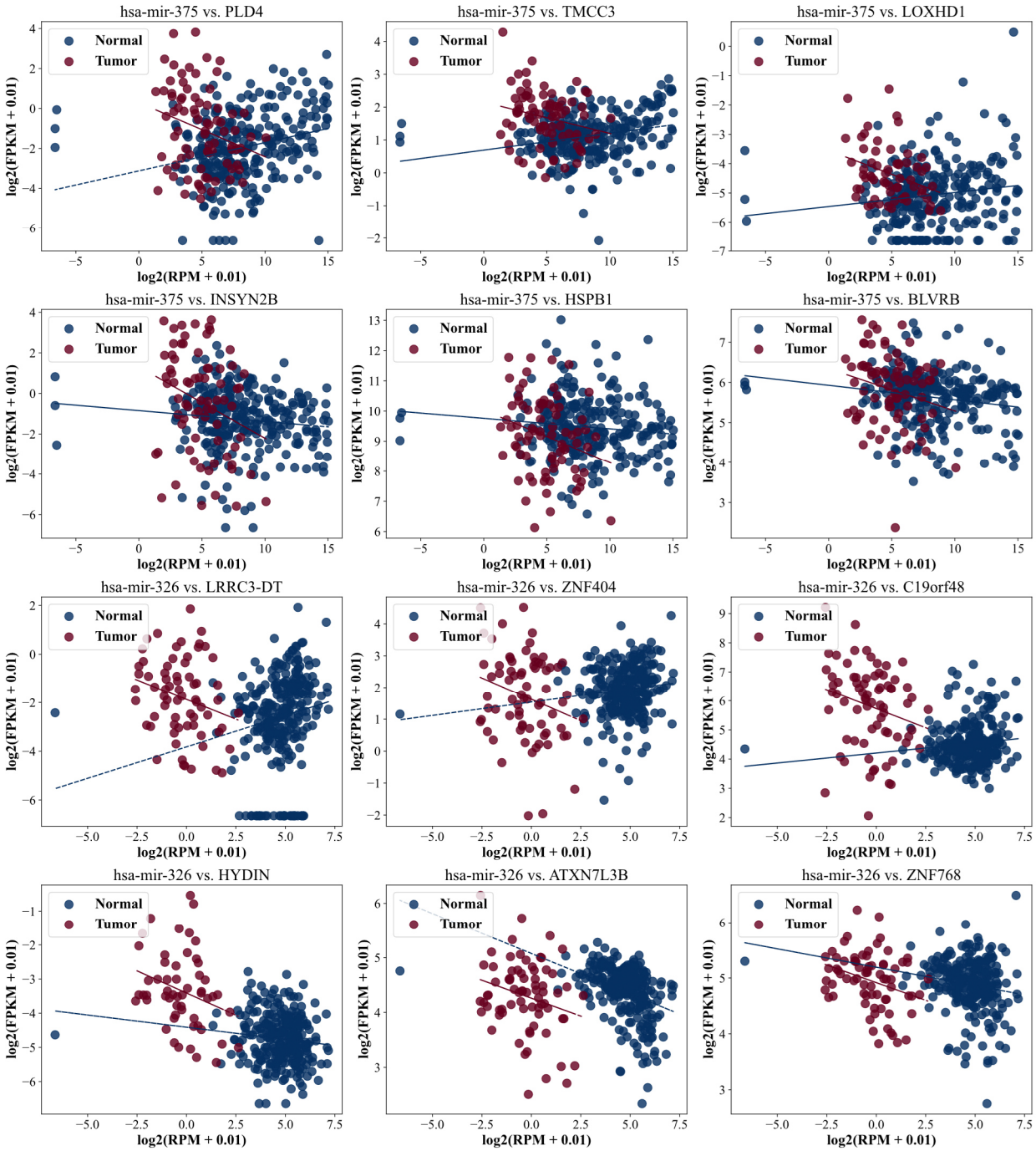

Figure 4. Scatter plots illustrating representative miRNA–mRNA pairs for miR-375 and miR-326 that exhibit a reversal in correlation direction or substantial Δr between normal (GTEx 2025 [30]) and tumor (TCGA-ACC [29]) samples, highlighting dynamic regulatory shifts in ACC.

3.5 Prognostic Value of Central miRNAs

Despite their central positions in the ceRNA regulatory network, miR-940, miR-375, and miR-326 did not individually demonstrate statistically significant associations with patient survival based

on Kaplan–Meier analysis, likely due to their post-transcriptional regulatory nature and the limited dynamic range of their expression. To overcome this limitation and indirectly assess their prognostic potential, survival outcomes were instead evaluated for selected key target genes of each miRNA, based on both validated interactions and biological relevance to tumor progression. Patients were stratified into high and low expression groups using the median cutoff ($n = 38$ per group), and Kaplan–Meier plots were generated using GEPIA2 [37] (Figure 5). The analysis focused on targets expected to be oncogenic if de-repressed, as would be the case with loss of tumor-suppressive miRNA regulation.

The survival data provided strong indirect evidence of tumor-suppressive activity for all three miRNAs. For miR-940, overexpression of targets such as CEP63, FRY, HEXB, and CPNE8 was associated with reduced overall survival (e.g., HR = 4.1 for HOXD3, $p = 0.00088$). Similarly, targets of miR-375 including HOXD3, JUND, LDHB, and RBM39 showed significant hazard ratios (HR > 2.5), supporting their oncogenic potential. For miR-326, targets such as SNRPB, DPF2, DYNLL1, and PNISR also exhibited strong survival associations, further reinforcing their role as biologically relevant effectors. These findings, visualized in Figure 5, highlight the inverse relationship between target gene overexpression and patient survival, collectively supporting the functional role of miR-940, miR-375, and miR-326 as putative tumor suppressors in ACC.

3.6 Functional Analysis of Central miRNAs Target Genes

Enrichment analysis of the combined target genes of miR-940, miR-375, and miR-326 was performed using the DIANA-miRPath platform [38], revealing a set of significantly overrepresented biological pathways associated with tumor suppression. The results, summarized in Figure 6, show strong enrichment ($p < 0.05$ across all terms) in pathways such as the MLL5-L complex, transcriptional repressor complex, innate immune response, cell death, and mitotic cell cycle regulation—all of which are recognized for their roles in suppressing tumor progression. Additional suppressed pathways include intrinsic apoptotic signaling, transforming growth factor beta receptor signaling, Fc-gamma receptor-mediated phagocytosis, and transcriptional corepressor activity, further supporting the notion that these miRNAs cooperatively regulate genes involved in key anti-oncogenic processes. The coordinated targeting of such pathways provides functional evidence consistent with the tumor-suppressive roles of these miRNAs in ACC.

To gain mechanistic insights into the biological roles of the target genes regulated by miR-940, miR-375, and miR-326, gene ontology (GO) enrichment analysis was conducted using the DAVID functional annotation platform [39]. GO terms were identified across the Biological Process (BP) category, with statistical significance thresholds of $p < 0.05$. The results, summarized in Table 5, reveal enrichment of pathways primarily associated with oncogenic hallmarks, providing indirect yet functional evidence of miRNA-mediated repression in ACC. Notably, miR-940 targets were enriched in processes such as cell adhesion, steroid hormone signaling, toll-like receptor signaling, and multiple forms of ubiquitination, all known to be implicated in cancer progression and immune

evasion. Similarly, targets of miR-375 were involved in transcriptional activation, epithelial cell proliferation, EGF signaling, and Wnt pathway regulation, underscoring their role in sustaining tumor growth. For miR-326, enriched GO terms included positive regulation of angiogenesis, cell migration, actin cytoskeleton remodeling, and DNA replication control, which are central to metastasis and cell cycle dysregulation.

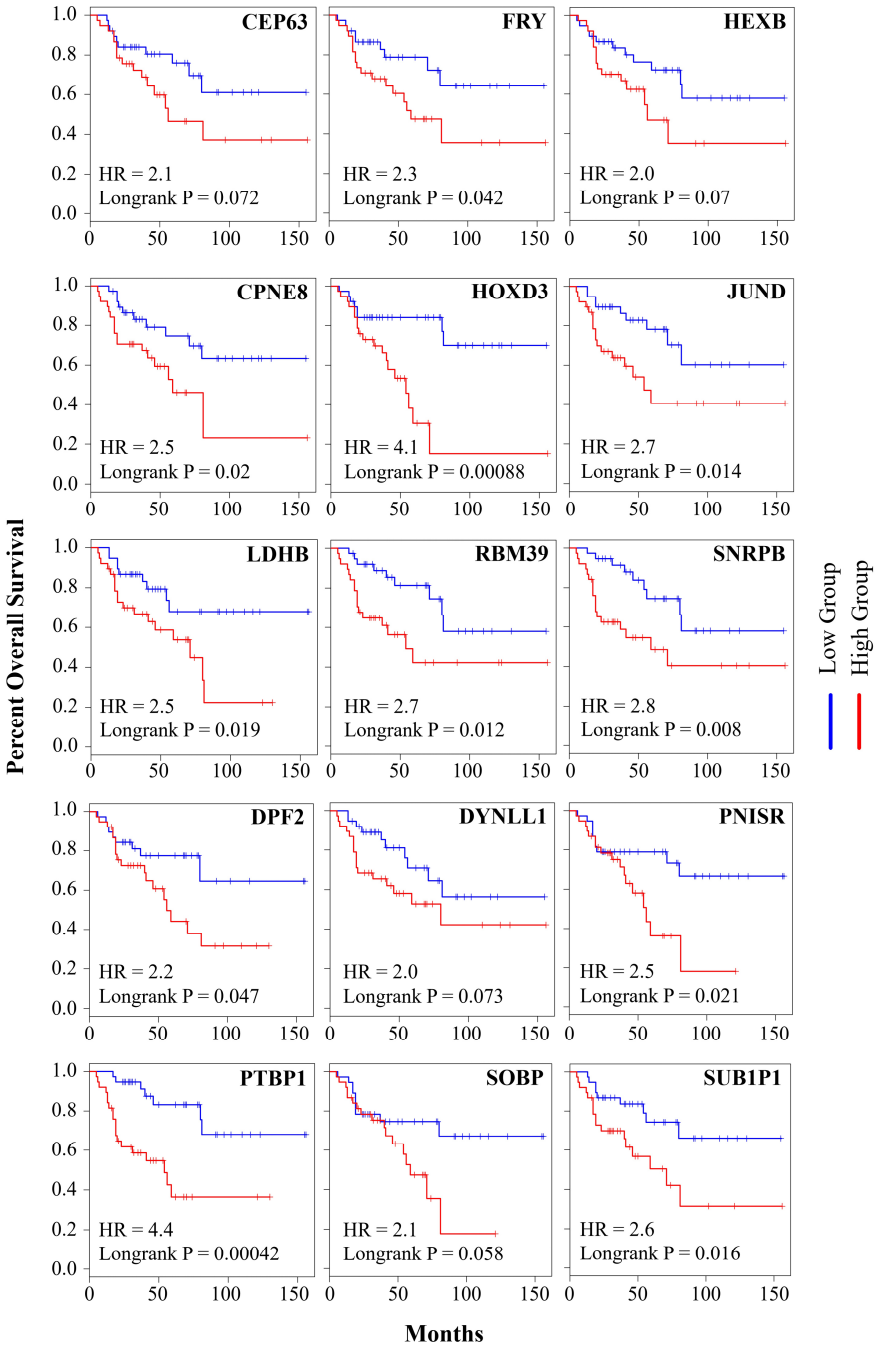

Figure 5. Kaplan–Meier survival GEPIA2 analyses [37] of central miRNAs' their key target genes in ACC. For each central miRNA, two biologically relevant target genes were selected based on validated

interactions and functional importance. Patients were stratified into high and low expression groups based on the median expression level (number of patients in the high group was 38, and in the low group was 38).

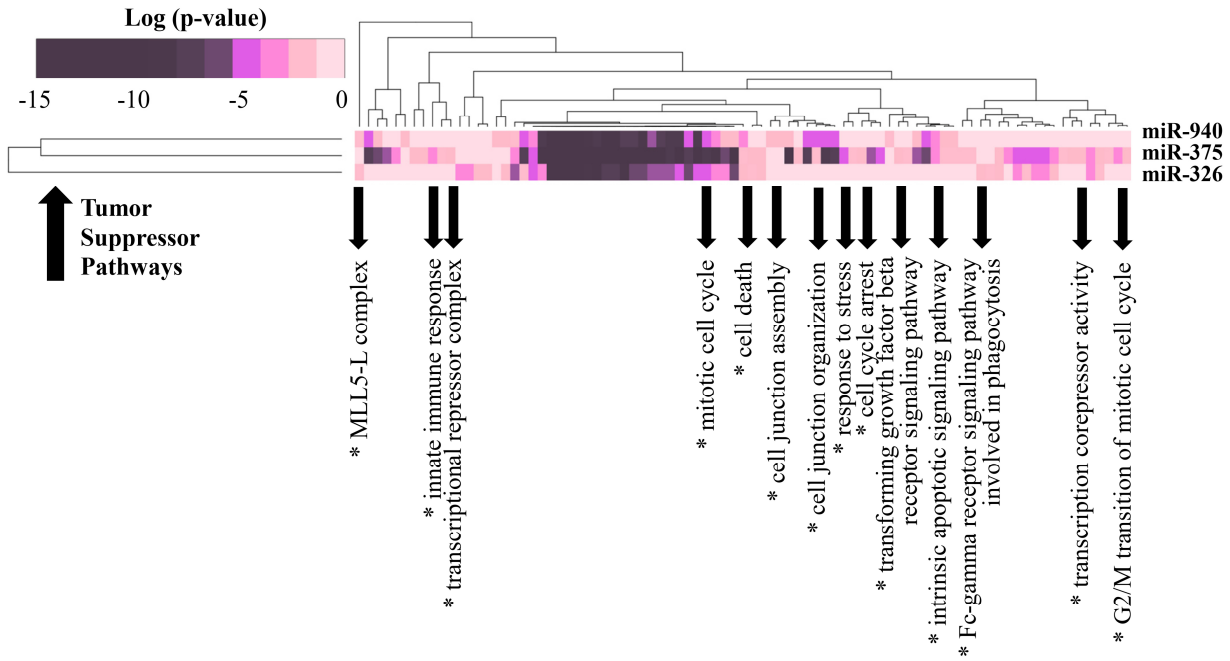

Figure 6. Hierarchical clustering of significantly enriched biological pathways based on DIANA-miRPath analysis [38] of target genes regulated by miR-940, miR-375, and miR-326. Highlighted pathways are associated with tumor-suppressive functions, supporting the coordinated regulatory role of these miRNAs in ACC.

These enriched biological functions suggest that the genes regulated by each miRNA are critically involved in processes that facilitate oncogenesis. The suppression of such genes by miR-940, miR-375, and miR-326 thus reinforces their functional classification as tumor-suppressive miRNAs in ACC. While the current discussion emphasizes BP categories, comprehensive GO profiling in Table 5 also includes significantly enriched Cellular Component (CC) and Molecular Function (MF) terms, many of which are likewise aligned with tumorigenic mechanisms, including chromatin-binding, transcriptional coactivator activity, and components of nuclear signaling complexes. Together, these data provide a coherent functional framework linking the regulatory activity of central miRNAs to the suppression of oncogenic programs in ACC. These findings are further illustrated in Figure 7, which visualizes the GO term enrichment profiles of each miRNA across Biological Process (BP), Cellular Component (CC), and Molecular Function (MF) categories, highlighting the distinct and functionally relevant targeting patterns that underpin their tumor-suppressive potential in ACC.

Table 5. Enriched GO terms associated with three central miRNAs of miR-940, miR-375, miR-326 using the DAVID functional annotation platform [39]; only significantly enriched pathways (P-value < 0.05) which are relevant to cancer are reported.

Central miRNA	Term	Category	Count	P-Value	Fold Enrichment
miR-940	GO:0085020~protein K6-linked ubiquitination	BP	4	0.00566	10.70808
miR-940	GO:0032482~Rab protein signal transduction	BP	4	0.00566	10.70808
miR-940	GO:0034220~monoatomic ion transmembrane transport	BP	9	0.013662	2.864225
miR-940	GO:0051865~protein autoubiquitination	BP	6	0.019756	3.84586
miR-940	GO:0050821~protein stabilization	BP	12	0.020251	2.219968
miR-940	GO:0007155~cell adhesion	BP	21	0.02197	1.709653
miR-940	GO:0072488~ammonium transmembrane transport	BP	3	0.023135	12.41164
miR-940	GO:0030518~nuclear receptor-mediated steroid hormone signaling pathway	BP	4	0.025067	6.277151
miR-940	GO:0044314~protein K27-linked ubiquitination	BP	3	0.027365	11.37734
miR-940	GO:0002755~MyD88-dependent toll-like receptor signaling pathway	BP	3	0.04698	8.533002
miR-940	GO:0030001~metal ion transport	BP	3	0.04698	8.533002
miR-940	GO:0000122~negative regulation of transcription by RNA polymerase II	BP	30	0.049779	1.425136
miR-940	GO:0031966~mitochondrial membrane	CC	14	3.55E-04	3.298699
miR-940	GO:0030054~cell junction	CC	13	0.001243	3.047608
miR-940	GO:0010008~endosome membrane	CC	16	0.001732	2.54342
miR-940	GO:0005886~plasma membrane	CC	149	0.002001	1.235697
miR-940	GO:0005789~endoplasmic reticulum membrane	CC	38	0.015066	1.487236
miR-940	GO:0045121~membrane raft	CC	11	0.016243	2.419865
miR-940	GO:0005794~Golgi apparatus	CC	36	0.017756	1.489329
miR-940	GO:0042995~cell projection	CC	11	0.022244	2.299962
miR-940	GO:0005743~mitochondrial inner membrane	CC	19	0.02733	1.732673
miR-940	GO:0005923~bicellular tight junction	CC	8	0.029771	2.690864
miR-940	GO:0005515~protein binding	MF	342	3.10E-04	1.10315
miR-940	GO:0004842~ubiquitin-protein transferase activity	MF	15	9.65E-04	2.818612
miR-940	GO:0035091~phosphatidylinositol binding	MF	8	0.014274	3.126248
miR-940	GO:0031624~ubiquitin conjugating enzyme binding	MF	4	0.029614	5.887768
miR-375	GO:0045893~positive regulation of DNA-templated transcription	BP	34	1.31E-06	2.576455
miR-375	GO:0045944~positive regulation of transcription by RNA polymerase II	BP	44	2.57E-05	1.975639
miR-375	GO:0043066~negative regulation of apoptotic process	BP	25	3.36E-05	2.626483
miR-375	GO:0006357~regulation of transcription by RNA polymerase II	BP	55	6.58E-05	1.73922
miR-375	GO:0071364~cellular response to epidermal growth factor stimulus	BP	7	1.89E-04	8.233454
miR-375	GO:0010467~gene expression	BP	13	2.55E-04	3.644416
miR-375	GO:0035019~somatic stem cell population maintenance	BP	7	6.18E-04	6.644542
miR-375	GO:1904262~negative regulation of TORC1 signaling	BP	6	0.002875	6.125157
miR-375	GO:0006479~protein methylation	BP	4	0.003485	12.73072
miR-375	GO:0006338~chromatin remodeling	BP	24	0.004446	1.892906
miR-375	GO:2001237~negative regulation of extrinsic apoptotic signaling pathway	BP	5	0.00511	7.119152
miR-375	GO:0060736~prostate gland growth	BP	3	0.006691	23.1881
miR-375	GO:0050679~positive regulation of epithelial cell proliferation	BP	6	0.009413	4.637619
miR-375	GO:0010628~positive regulation of gene expression	BP	18	0.009858	1.991616
miR-375	GO:0051897~positive regulation of phosphatidylinositol 3-kinase/protein kinase B signal transduction	BP	10	0.013659	2.652233
miR-375	GO:0060070~canonical Wnt signaling pathway	BP	7	0.013743	3.573008

miR-375	GO:0050673~epithelial cell proliferation	BP	5	0.01436	5.304466
miR-375	GO:0005654~nucleoplasm	CC	128	1.95E-11	1.75163
miR-375	GO:0000785~chromatin	CC	43	5.32E-06	2.133024
miR-375	GO:0005667~transcription regulator complex	CC	15	4.82E-05	3.780451
miR-375	GO:0005634~nucleus	CC	144	1.87E-04	1.296155
miR-375	GO:0090575~RNA polymerase II transcription regulator complex	CC	10	4.21E-04	4.460532
miR-375	GO:0016604~nuclear body	CC	17	0.0013	2.520966
miR-375	GO:0016323~basolateral plasma membrane	CC	12	0.009188	2.497898
miR-375	GO:0031463~Cul3-RING ubiquitin ligase complex	CC	5	0.020654	4.762941
miR-375	GO:0005739~mitochondrion	CC	43	0.022008	1.404251
miR-375	GO:0017053~transcription repressor complex	CC	5	0.023044	4.606779
miR-375	GO:0000791~euchromatin	CC	5	0.026931	4.390836
miR-375	GO:0016363~nuclear matrix	CC	7	0.029541	3.003198
miR-375	GO:0035525~NF-kappaB p50/p65 complex	CC	2	0.035175	56.2027
miR-375	GO:0033276~transcription factor TFTC complex	CC	3	0.039841	9.367117
miR-375	GO:0000976~transcription cis-regulatory region binding	MF	17	1.32E-05	3.762037
miR-375	GO:0003700~DNA-binding transcription factor activity	MF	28	3.45E-05	2.448045
miR-375	GO:0000978~RNA polymerase II cis-regulatory region sequence-specific DNA binding	MF	40	3.74E-04	1.814028
miR-375	GO:0000981~DNA-binding transcription factor activity, RNA polymerase II-specific	MF	42	3.77E-04	1.780573
miR-375	GO:0001228~DNA-binding transcription activator activity, RNA polymerase II-specific	MF	22	4.69E-04	2.360791
miR-375	GO:1990837~sequence-specific double-stranded DNA binding	MF	23	0.001095	2.159587
miR-375	GO:0003677~DNA binding	MF	46	0.001119	1.635527
miR-375	GO:0003682~chromatin binding	MF	20	0.002396	2.1724
miR-375	GO:0004674~protein serine/threonine kinase activity	MF	17	0.002447	2.367235
miR-375	GO:0061629~RNA polymerase II-specific DNA-binding transcription factor binding	MF	11	0.002497	3.188351
miR-375	GO:0106310~protein serine kinase activity	MF	16	0.003822	2.337859
miR-326	GO:0016477~cell migration	BP	15	0.001479	2.695295
miR-326	GO:0045766~positive regulation of angiogenesis	BP	11	0.001821	3.326988
miR-326	GO:0006275~regulation of DNA replication	BP	6	0.001981	6.640227
miR-326	GO:0030036~actin cytoskeleton organization	BP	13	0.002339	2.826049
miR-326	GO:0006897~endocytosis	BP	11	0.007339	2.732883
miR-326	GO:0007015~actin filament organization	BP	9	0.010132	3.022448
miR-326	GO:0006357~regulation of transcription by RNA polymerase II	BP	50	0.010518	1.422998
miR-326	GO:0060395~SMAD protein signal transduction	BP	4	0.011146	8.468696
miR-326	GO:0051726~regulation of cell cycle	BP	12	0.01121	2.424647
miR-326	GO:0045893~positive regulation of DNA-templated transcription	BP	25	0.012368	1.705007
miR-326	GO:0005789~endoplasmic reticulum membrane	CC	42	3.51E-04	1.791768
miR-326	GO:0032587~ruffle membrane	CC	8	0.004084	3.968322
miR-326	GO:0030027~lamellipodium	CC	11	0.004749	2.913912
miR-326	GO:0070062~extracellular exosome	CC	62	0.005909	1.399179
miR-326	GO:0005654~nucleoplasm	CC	99	0.020949	1.219629
miR-326	GO:0005741~mitochondrial outer membrane	CC	10	0.036667	2.228903
miR-326	GO:0030054~cell junction	CC	9	0.043078	2.299823
miR-326	GO:0031982~vesicle	CC	8	0.044292	2.468103
miR-326	GO:0005515~protein binding	MF	318	3.30E-06	1.14087
miR-326	GO:0003925~G protein activity	MF	6	0.006389	5.080841
miR-326	GO:0045296~cadherin binding	MF	14	0.013916	2.155508
miR-326	GO:0031267~small GTPase binding	MF	13	0.017136	2.179155
miR-326	GO:0035064~methylated histone binding	MF	6	0.017293	3.982281
miR-326	GO:0106310~protein serine kinase activity	MF	15	0.017664	2.018416

miR-326	GO:0036408~histone H3K14 acetyltransferase activity	MF	4	0.020546	6.774455
miR-326	GO:0043996~histone H4K8 acetyltransferase activity	MF	4	0.024537	6.337393
miR-326	GO:0043997~histone H4K12 acetyltransferase activity	MF	4	0.024537	6.337393
miR-326	GO:0043995~histone H4K5 acetyltransferase activity	MF	4	0.024537	6.337393
miR-326	GO:0004705~JUN kinase activity	MF	3	0.031863	10.5246
miR-326	GO:0004707~MAP kinase activity	MF	3	0.03628	9.822959
miR-326	GO:0005178~integrin binding	MF	8	0.045185	2.45574

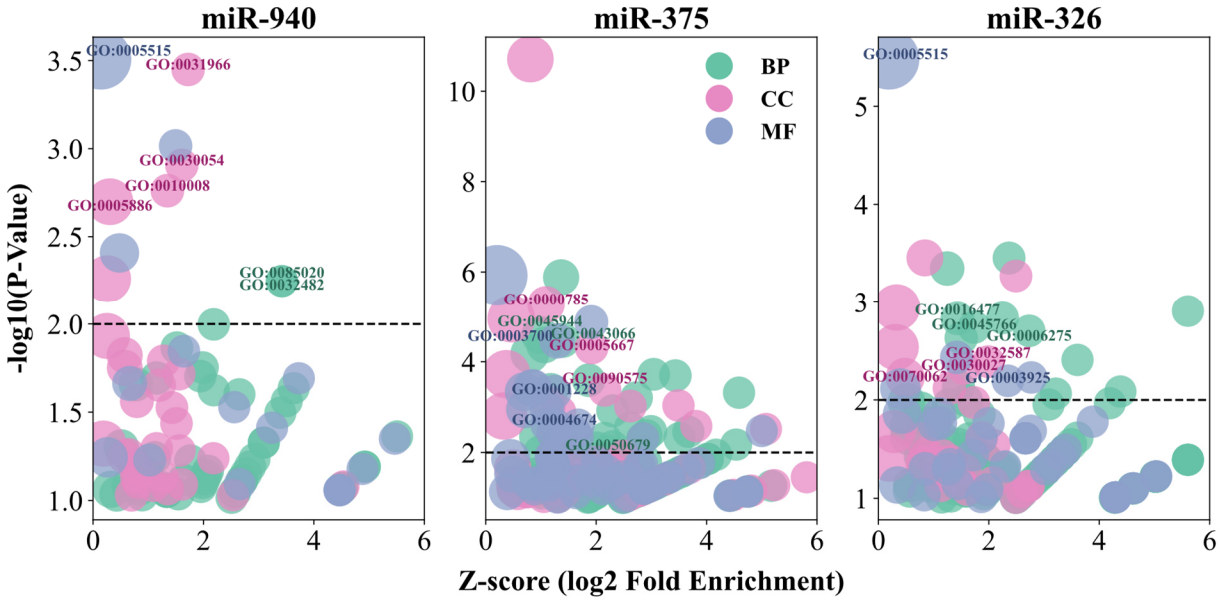

Figure 7. GO enrichment bubble plot for miR-940, miR-375, miR-326 using the DAVID functional annotation platform [39]; colors represent GO categories (green: Biological Process, orange: Cellular Component, blue: Molecular Function). Bubble size indicates the number of associated genes, and the dashed line denotes the significance threshold of 2.

To further elucidate the functional relevance of the target genes, Reactome pathway enrichment analysis using the DAVID functional annotation platform [39] was performed individually for miR-940, miR-375, and miR-326. The analysis revealed significant enrichment ($p < 0.05$) of oncogenic signaling pathways across all three miRNA target sets, as summarized in Table 6. For miR-940, pathways such as cell-cell junction organization, adherens junction interactions, and the RHOJ GTPase cycle were identified, which are known to be dysregulated during tumor invasion and metastasis. miR-375 targets were enriched in pathways including transcriptional activation, ERBB2 signaling, TP53 regulation, and PI3K/Akt signaling, all of which are critically involved in proliferation and evasion of apoptosis. Likewise, miR-326 target genes mapped to highly cancer-associated pathways such as Rho GTPase signaling, NTRK signaling, TP53 acetylation, and extracellular matrix organization, each contributing to aggressive tumor behavior when upregulated. Collectively, these findings provide functional evidence that the repression of these oncogenic pathways by miR-940, miR-375, and miR-326 is consistent with a tumor-suppressive role in ACC. The graphical representation of these pathway enrichments is provided in Figure 8,

where bubble size indicates gene counts and the dashed line marks the statistical significance threshold.

Table 6. Enriched Reactome pathways associated with the target genes of the three central miRNAs of miR-940, miR-375, miR-326 using the DAVID functional annotation platform [39]; only significantly enriched pathways (P-value < 0.05) which are relevant to cancer are reported to ensure biological specificity and statistical confidence.

Central miRNA	Term	Count	P-Value	Fold Enrichment
miR-940	R-HSA-421270~Cell-cell junction organization	8	0.004788	3.82655
miR-940	R-HSA-9013409~RHOJ GTPase cycle	6	0.009069	4.64404
miR-940	R-HSA-446728~Cell junction organization	8	0.019112	2.935888
miR-940	R-HSA-1500931~Cell-Cell communication	9	0.027386	2.504139
miR-940	R-HSA-418990~Adherens junctions interactions	5	0.04408	3.734243
miR-375	R-HSA-74160~Gene expression (Transcription)	56	0.001562	1.53977
miR-375	R-HSA-8939211~ESR-mediated signaling	14	0.002097	2.786087
miR-375	R-HSA-212436~Generic Transcription Pathway	45	0.002296	1.576185
miR-375	R-HSA-9006934~Signaling by Receptor Tyrosine Kinases	24	0.004164	1.979705
miR-375	R-HSA-2032785~YAP1- and WWTR1 (TAZ)-stimulated gene expression	4	0.019854	11.83423
miR-375	R-HSA-9839394~TGFBR3 expression	4	0.021974	6.827443
miR-375	R-HSA-389357~CD28 dependent PI3K/Akt signaling	4	0.033642	6.574575
miR-375	R-HSA-3700989~Transcriptional Regulation by TP53	15	0.048973	1.843977
miR-375	R-HSA-9665348~Signaling by ERBB2 ECD mutants	3	0.04962	8.320946
miR-375	R-HSA-6806003~Regulation of TP53 Expression and Degradation	4	0.001562	4.797663
miR-326	R-HSA-373755~Semaphorin interactions	7	0.004361	4.515039
miR-326	R-HSA-162582~Signal Transduction	81	0.004966	1.3121
miR-326	R-HSA-9664565~Signaling by ERBB2 KD Mutants	4	0.01993	6.811259
miR-326	R-HSA-9716542~Signaling by Rho GTPases, Miro GTPases and RHOBTB3	27	0.021691	1.570219
miR-326	R-HSA-1227990~Signaling by ERBB2 in Cancer	4	0.022149	6.549288
miR-326	R-HSA-194315~Signaling by Rho GTPases	26	0.029254	1.545851
miR-326	R-HSA-1227986~Signaling by ERBB2	5	0.031045	4.173566
miR-326	R-HSA-6804758~Regulation of TP53 Activity through Acetylation	4	0.035172	5.492951
miR-326	R-HSA-166520~Signaling by NTRKs	8	0.036683	2.560624
miR-326	R-HSA-1474244~Extracellular matrix organization	14	0.040596	1.845155
miR-326	R-HSA-8849471~PTK6 Regulates RHO GTPases, RAS GTPase and MAP kinases	3	0.041261	9.122222
miR-326	R-HSA-187687~Signalling to ERKs	4	0.041271	5.160045
miR-326	R-HSA-1483255~PI Metabolism	6	0.048911	3.004967

Protein–protein interaction (PPI) networks were constructed using the STRING database [40] to investigate the functional interrelationships among the target genes of miR-940, miR-375, and miR-326, based on Reactome-enriched gene sets. Medium-confidence thresholds were applied (0.4 for miR-940 and miR-326; 0.3 for miR-375) to ensure a balance between sensitivity and specificity. As shown in Figure 9, the resulting networks revealed distinct topological features: the miR-940 network (pink) displayed a spoke-like structure with central nodes; the miR-375 network (blue) was organized around tightly connected hubs; and the miR-326 network (green) formed multiple interconnected clusters, reflecting modular architecture. Quantitative parameters summarizing these networks are reported in Table 7, including the number of nodes and edges, PPI enrichment p-values, average node degree (restricted to query genes), and average local

clustering coefficients. The observed connectivity patterns suggest that these miRNAs exert coordinated regulatory control over oncogenic protein modules, further supporting their tumor-suppressive roles in the molecular landscape of ACC. Although the STRING-derived networks for miR-940 and miR-375 did not reach formal significance in PPI enrichment, structural metrics such as clustering and node connectivity still revealed biologically relevant modules.

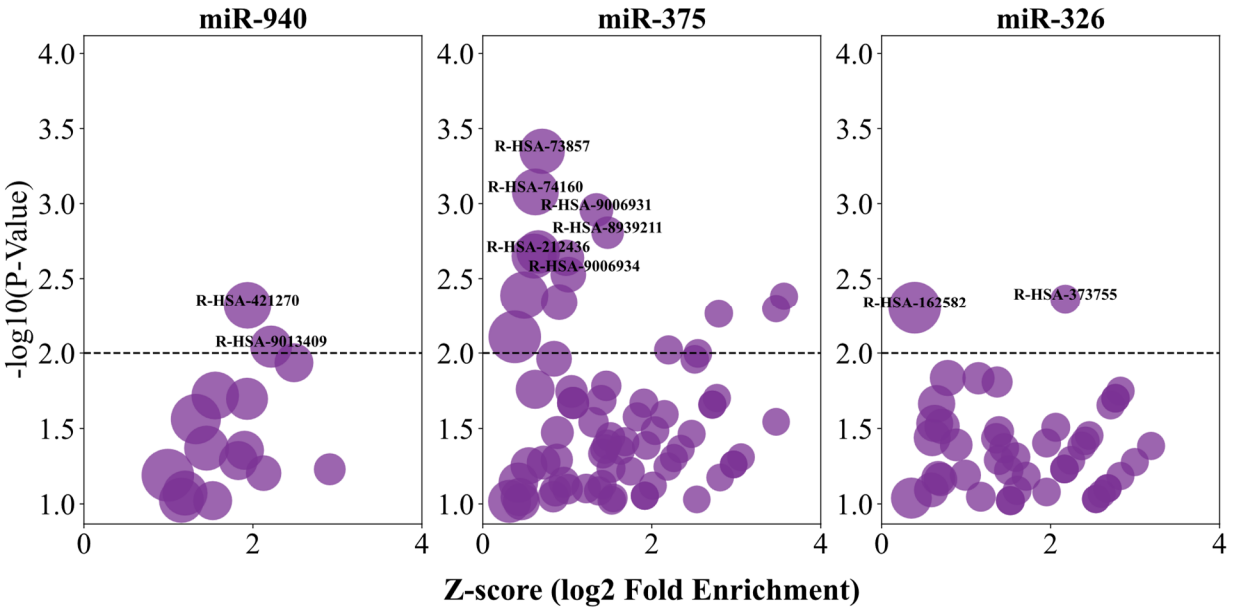

Figure 8. Reactome pathway enrichment bubble plot for miR-940, miR-375, and miR-326 using the DAVID functional annotation platform [39]. Colors represent distinct functional categories of Reactome pathways. Bubble size indicates the number of associated genes, and the dashed line marks the significance threshold of 2.

3.7 Therapeutic Implications

Expression dynamics of miR-940, miR-375, and miR-326 were investigated under different therapeutic regimens to assess their potential treatment-related regulation in ACC. Tumor miRNA expression data and clinical metadata were obtained from TCGA-ACC [29], and patients were stratified into two cohorts based on treatment modality: those receiving pharmaceutical therapy alone, and those receiving pharmaceutical therapy combined with radiation (hereafter referred to as the radiation group). To address distributional disparities between treatment arms, min–max normalization was applied within each group. The mean normalized expression values were then compared across the two cohorts by computing Δ values (Δ = mean_pharma − mean_radiation) for each miRNA, capturing the direction and magnitude of expression shift.

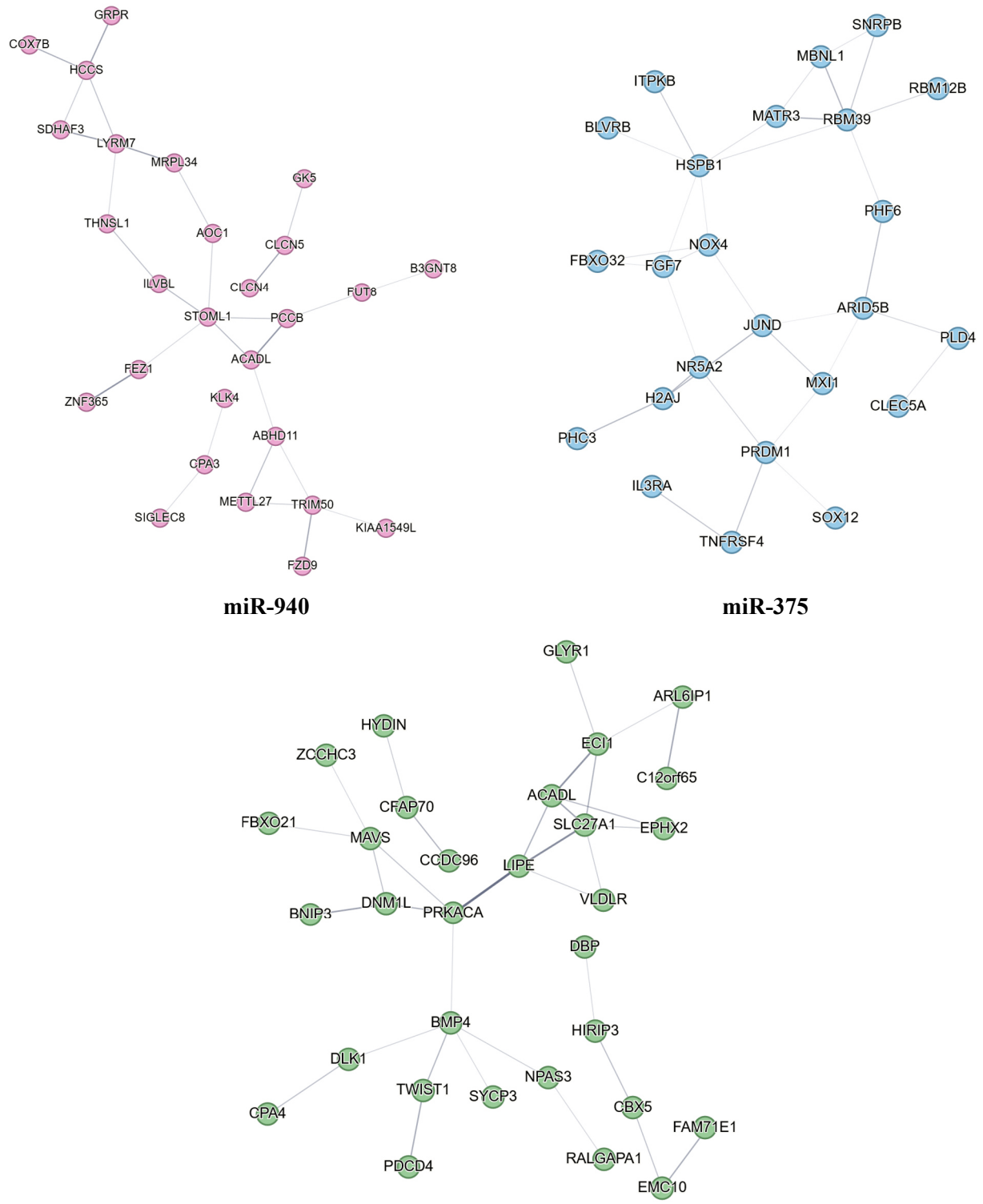

Figure 9. Protein–protein interaction (PPI) network of genes targeted by miR-940, miR-375, and miR-326 using STRING Platform [40]; (Medium confidence: miR-940: 0.4, miR-375: 0.3, miR-326: 0.4)

Table 7. Network topology parameters for PPI networks constructed from target genes of miR-940, miR-375, and miR-326 based on Reactome-enriched pathways.

miRNA	No. of Nodes	No. of Edges	PPI Enrichment p-value	Average Node Degree (Query Genes Only)	Average Local Clustering Coefficient
miR-940	109	42	0.269	0.771	0.281
miR-375	47	35	0.0939	1.49	0.340
miR-326	88	46	0.058	1.05	0.364

The resulting distribution of Δ values is shown in Figure 10a, where each bar represents a single miRNA's expression change between treatment groups. Notably, miR-940 exhibited a substantial negative Δ, indicating decreased expression in the pharmaceutical group compared to radiation. Conversely, miR-326 and miR-375 showed slightly elevated expression in pharmaceutical-treated patients, though the differences were modest. These trends were further confirmed in the radar plot (Figure 10b), which visualizes average expression levels across groups. A clear divergence in miR-940 expression was observed, with higher levels under radiation therapy, while miR-375 and miR-326 demonstrated comparable or slightly higher expression in pharmaceutical-only patients. These patterns suggest that miR-940 may exhibit radiation-sensitive expression, aligning with its proposed tumor-suppressive function and supporting its relevance in radiation-modulated regulatory programs.

Direct comparison of raw expression profiles is provided in Figure 11, where $\log_{10}$-transformed expression levels of the three miRNAs are plotted across the two treatment groups. miR-940 displayed significantly reduced expression in the pharmaceutical group relative to radiation, further emphasizing its differential responsiveness to therapy. For miR-375, slightly higher expression was noted under radiation therapy, whereas miR-326 showed relatively uniform expression across both conditions. These observations collectively suggest that miR-940 may represent a radiation-responsive tumor suppressor, while miR-375 and miR-326 exhibit more stable or pharmacologically influenced expression patterns, offering additional insights into the context-specific regulatory dynamics of central miRNAs in ACC treatment.

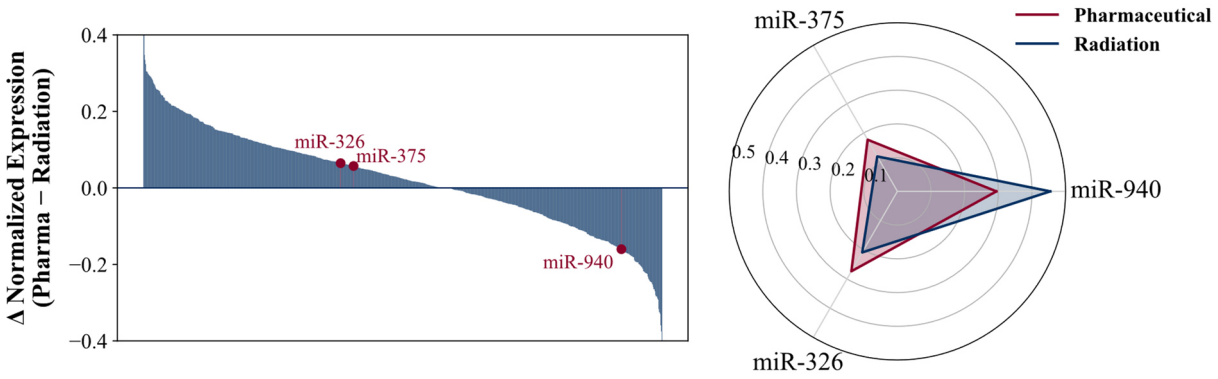

(a) (b)

Figure 10. Differential expression analysis of miR-940, miR-375, and miR-326 across treatment groups. (a) Waterfall plot showing Δ normalized expression values (pharmaceutical − radiation) for all expressed miRNAs, highlighting the three central miRNAs. (b) Radar plot comparing average normalized expression levels between pharmaceutical and radiation therapy groups.

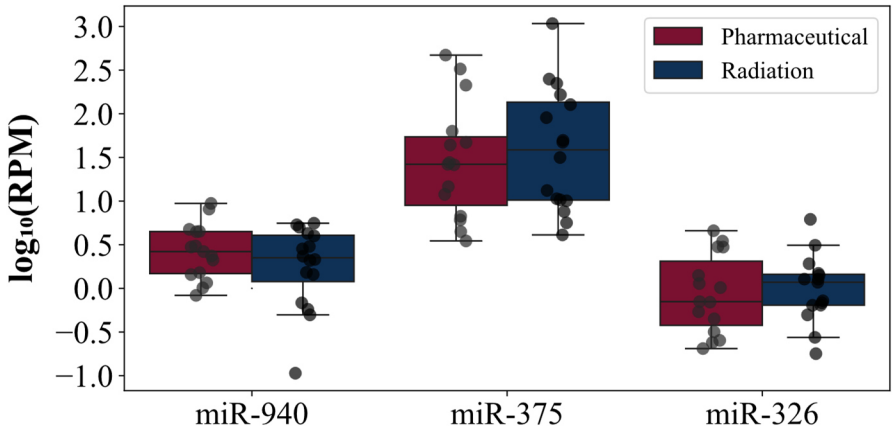

Figure 11. Log-transformed expression levels of selected miRNAs (miR-940, miR-375, and miR-326) across two treatment groups in ACC tumor samples. Boxplots compare the $\log_{10}$-transformed expression values (excluding zero-expression samples) between patients who received pharmaceutical therapy (red) and those who underwent radiation therapy (blue).

3.8 Cross-Cancer Expression Analysis of Central miRNAs

Cross-cancer expression profiles of miR-940, miR-375, and miR-326 were assessed using TCGA-derived RNA-seq data [29] across multiple tumor types, comparing tumor and normal tissues. The results, illustrated in Figure 12, reveal distinct expression patterns suggestive of context-specific regulatory roles for each miRNA. Notably, miR-940 exhibited reduced expression in tumor tissues relative to normal in THCA, COAD, and READ, indicative of tumor-suppressive role in these cancers. A broader suppressive pattern was observed for miR-375, which showed significantly lower expression in tumors from KIRC, HNSC, LUSC, SKCM, COAD, LIHC, ESCA, and READ. In contrast, miR-326 demonstrated the most widespread downregulation, with tumor-specific reduction evident in BRCA, UCEC, KIRC, HNSC, THCA, LUSC, PRAD, COAD, STAD, BLCA, LIHC, KIRP, ESCA, READ, THYM, and KICH, supporting its broad tumor-suppressive potential across cancers. Among these, the expression trends observed in COAD and READ most closely mirrored those seen in ACC, suggesting that the regulatory dynamics of these three miRNAs in ACC may be particularly similar to those operative in colorectal malignancies.

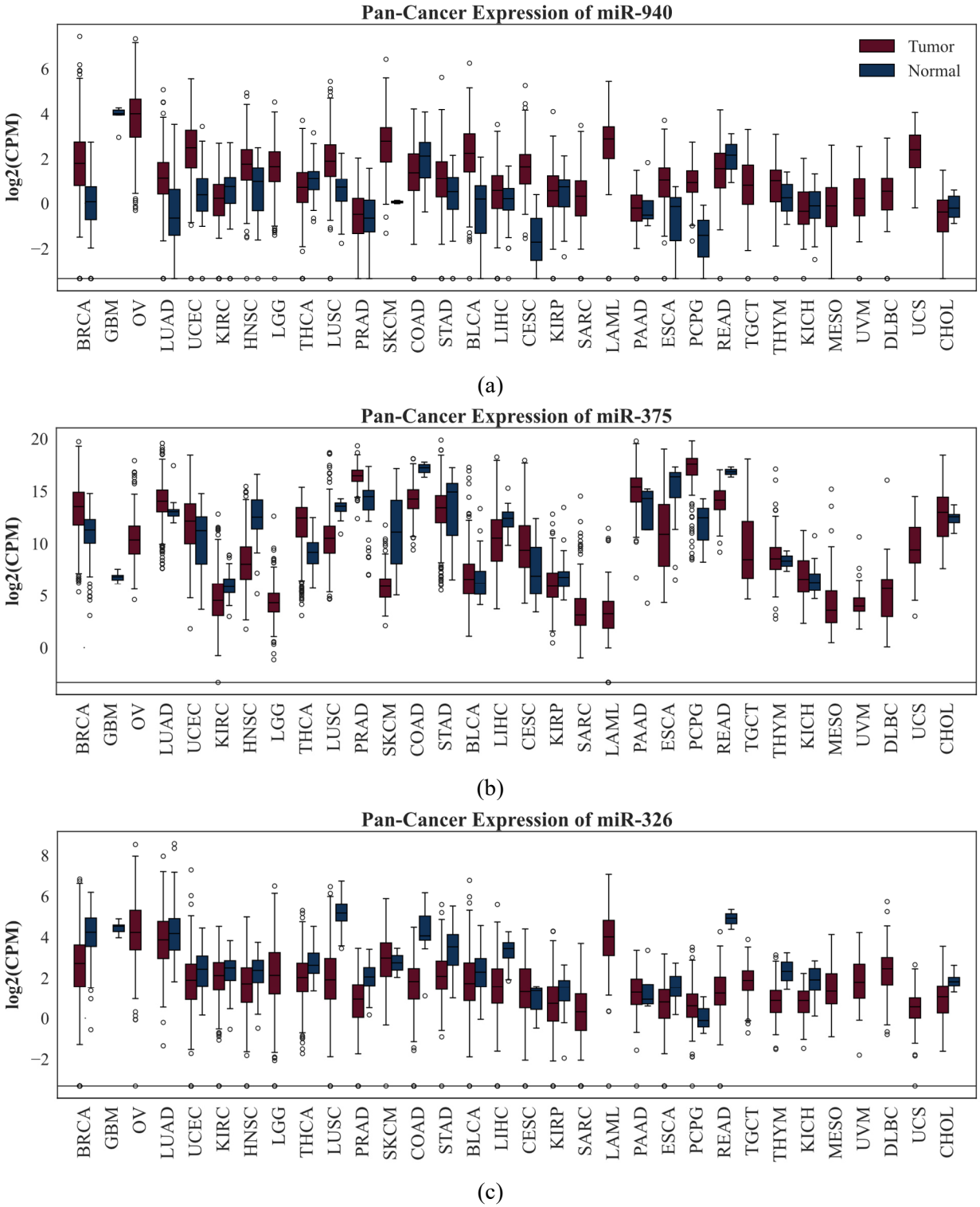

Figure 12. Pan-cancer expression profiles of (a) miR-940, (b) miR-375, and (c) miR-326 across TCGA tumor types [29]. Boxplots display $\log_2$(CPM) values comparing tumor (red) and normal (blue) tissues.

3.8 Discussion and Future Works

In this study, miR-940, miR-375, and miR-326 were characterized as context-dependent tumor suppressors within the ceRNA landscape of adrenocortical carcinoma (ACC), providing the first integrative evidence of their regulatory prominence in this rare endocrine malignancy. To the best of our knowledge, this is the first integrative study to characterize the tumor-suppressive roles and regulatory centrality of miR-940, miR-375, and miR-326 in adrenocortical carcinoma using a ceRNA network-based systems biology approach.

The findings related to miR-940 are consistent with earlier reports on other cancer types. In hepatocellular carcinoma, overexpression of miR-940 was found to inhibit cell growth, migration, and invasion, primarily through repression of CXCR2 [19]. Similarly, in esophageal squamous cell carcinoma, it was reported that miR-940 restoration suppressed proliferation and induced apoptosis via downregulation of SRCIN1, supporting a tumor-suppressive function [20]. In triple-negative breast cancer, miR-940 was shown to target ZNF24 and reduce oncogenic activity [21]. These observations parallel the current study, where miR-940 emerged as a tumor-specific hub in the ACC ceRNA network, displaying significant negative correlations with multiple oncogenic targets and showing increased expression in radiation-treated patients, suggesting a responsive regulatory mechanism under therapeutic pressure.

MiR-375 has similarly been characterized as a tumor suppressor in various malignancies. In oral squamous cell carcinoma, Jung et al. demonstrated that miR-375 repressed CIP2A and destabilized MYC, thereby reducing proliferation and invasion [24]. A systematic review [22] emphasized the broad inhibitory roles of miR-375 across gastric, hepatic, and lung cancers, noting its impact on epithelial–mesenchymal transition and resistance pathways. Additionally, miR-375 has been shown to repress the RON oncogene and induce G1 cell cycle arrest in gastric cancer [23]. In prostate cancer, miR-375 was found to suppress migration and invasion in both AR-positive and AR-negative cells, forming a central node in ceRNA-based networks associated with aggressive disease [25]. These findings are congruent with the current observation that miR-375 lost centrality in the tumor-specific ACC network despite being highly expressed in normal adrenal tissue, reinforcing its role as a repressed regulatory element during tumorigenesis.

MiR-326 has also been extensively documented as a tumor suppressor. In colorectal cancer, it was shown to inhibit cell proliferation, migration, and invasion by targeting NOB1 [28]. Similar findings were reported in non-small-cell lung cancer, where miR-326 repressed the oncogenic transcription factor SP1 and suppressed EMT [27]. In prostate carcinoma, miR-326 reduced proliferation and metastasis through MUC1 regulation and modulated the PI3K/AKT pathway [26]. The present study confirms and extends these insights by positioning miR-326 as a central node in the normal adrenal ceRNA network and documenting its significant loss of centrality in tumor samples, consistent with oncogenic suppression. Furthermore, several targets of miR-326 exhibited dynamic correlation shifts between normal and tumor states, highlighting context-

dependent regulatory rewiring and suggesting that the integrative analytical framework used in this study may be applicable to other rare cancers for systematic discovery of non-coding RNA-based regulatory programs.

Together, these cross-cancer comparisons support the notion that miR-940, miR-375, and miR-326 belong to a conserved class of tumor-suppressive miRNAs that are actively downregulated or functionally suppressed in cancer-specific ceRNA networks. The novelty of the current work lies in uncovering their regulatory role in ACC, where their expression profiles, network topologies, correlation reversals, and target enrichment analyses collectively support their suppressive influence on oncogenic programs.

Despite these insights, additional research is required to confirm and extend these findings. Functional validation through in vitro assays and in vivo models is necessary to establish the causal role of these miRNAs in ACC tumorigenesis. The specific regulatory impact of each miRNA on their negatively correlated oncogenic targets, such as HOXD3, LDHB, and SNRPB, should be experimentally dissected through loss- and gain-of-function studies in ACC cell lines. Furthermore, therapeutic modulation of these miRNAs using mimics or nanoparticle delivery systems may offer promising avenues for future interventions. The observed therapy-responsive behavior of miR-940 particularly merits further investigation, as its upregulation following radiation suggests a potential role as a predictive biomarker for treatment response.

Given the context-specific nature of miRNA activity, exploration of the upstream regulatory mechanisms that drive their suppression in ACC may also be valuable. Epigenetic silencing, ceRNA competition, or dysregulation of miRNA-processing enzymes could each contribute to the observed loss of centrality and expression. Finally, pan-cancer profiling highlighted a shared pattern of downregulation for all three miRNAs in colorectal and thyroid malignancies, suggesting broader applicability for their use as diagnostic or prognostic indicators.

In summary, while miR-940, miR-375, and miR-326 have been well-studied in other cancers, their tumor-suppressive roles in adrenocortical carcinoma were identified for the first time in this study. The integration of ceRNA network topology, correlation-based filtering, differential expression analysis, and functional enrichment supports their central roles in ACC progression and underscores their potential as both therapeutic and prognostic tools, laying the groundwork for future translation of miRNA-based diagnostics or targeted therapeutics in the clinical management of ACC.

4. Conclusion

In this study, a comprehensive computational framework, leveraging a novel integrative analytical approach specifically developed in this study, was applied to investigate the tumor-suppressive roles of miR-940, miR-375, and miR-326 in adrenocortical carcinoma (ACC). Transcriptomic datasets from TCGA [29], GTEx 2025 [30], and miRNATissueAtlas 2025 [31] were integrated

and analyzed to construct competing endogenous RNA (ceRNA) networks representing both normal and tumor adrenal tissues. Through this approach, significant topological differences were identified between the two states, and a pronounced rewiring of post-transcriptional regulatory networks was observed in ACC.

Validated and predicted miRNA–mRNA interactions were evaluated, and significant negative correlations were identified between the three miRNAs and numerous upregulated oncogenes, including HOXD3, LDHB, and SNRPB. Several of these targets were found to be associated with poor survival, providing indirect evidence for the tumor-suppressive potential of the miRNAs. Additionally, context-specific regulatory shifts were observed through correlation reversal analyses, where targets switched from positive to negative correlation in tumor samples. Functional enrichment analyses revealed that target genes of miR-940, miR-375, and miR-326 are involved in key oncogenic processes such as transcriptional activation, cell proliferation, migration, immune response, and Wnt/PI3K signaling. These pathways were significantly enriched and were also reflected in protein–protein interaction networks, supporting the coordinated repression of oncogenic modules by the miRNAs. Moreover, treatment-related expression analysis indicated that miR-940 was upregulated in radiation-treated patients, suggesting a radiation-responsive regulatory response, while miR-375 and miR-326 showed stable or modest variation. Cross-cancer analysis confirmed that downregulation of these miRNAs is recurrent in other cancers, particularly colorectal and thyroid, suggesting broader relevance. In conclusion, miR-940, miR-375, and miR-326 were identified as context-dependent tumor suppressors in ACC, acting through the repression of oncogenic targets and pathways. Their potential for prognostic application and therapeutic targeting warrants further functional validation and translational research.

References

[1] Fassnacht, Martin, Matthias Kroiss, and Bruno Allolio. "Update in adrenocortical carcinoma." *The Journal of Clinical Endocrinology & Metabolism* 98, no. 12 (2013): 4551-4564.

[2] Else, Tobias, Alex C. Kim, Aaron Sabolch, Victoria M. Raymond, Asha Kandathil, Elaine M. Caoili, Shruti Jolly, Barbra S. Miller, Thomas J. Giordano, and Gary D. Hammer. "Adrenocortical carcinoma." *Endocrine reviews* 35, no. 2 (2014): 282-326.

[3] Libé, Rossella. "Adrenocortical carcinoma (ACC): diagnosis, prognosis, and treatment." *Frontiers in cell and developmental biology* 3 (2015): 45.

[4] Assié, Guillaume, Eric Letouzé, Martin Fassnacht, Anne Jouinot, Windy Luscap, Olivia Barreau, Hanin Omeiri et al. "Integrated genomic characterization of adrenocortical carcinoma." *Nature genetics* 46, no. 6 (2014): 607-612.

[5] Zheng, Siyuan, Andrew D. Cherniack, Ninad Dewal, Richard A. Moffitt, Ludmila Danilova, Bradley A. Murray, Antonio M. Lerario et al. "Comprehensive pan-genomic characterization of adrenocortical carcinoma." *Cancer cell* 29, no. 5 (2016): 723-736.

[6] Esteller, Manel. "Non-coding RNAs in human disease." *Nature reviews genetics* 12, no. 12 (2011): 861-874.

[7] Salmena, Leonardo, Laura Poliseno, Yvonne Tay, Lev Kats, and Pier Paolo Pandolfi. "A ceRNA hypothesis: the Rosetta Stone of a hidden RNA language?." *cell* 146, no. 3 (2011): 353-358.

[8] Liu, S. John, Ha X. Dang, Daniel A. Lim, Felix Y. Feng, and Christopher A. Maher. "Long noncoding RNAs in cancer metastasis." *Nature Reviews Cancer* 21, no. 7 (2021): 446-460.

[9] Kristensen, Lasse S., Maria S. Andersen, Lotte VW Stagsted, Karoline K. Ebbesen, Thomas B. Hansen, and Jørgen Kjems. "The biogenesis, biology and characterization of circular RNAs." *Nature reviews genetics* 20, no. 11 (2019): 675-691.

[10] Tay, Yvonne, John Rinn, and Pier Paolo Pandolfi. "The multilayered complexity of ceRNA crosstalk and competition." *Nature* 505, no. 7483 (2014): 344-352.

[11] Chiu, Hua-Sheng, Sonal Somvanshi, Ektaben Patel, Ting-Wen Chen, Vivek P. Singh, Barry Zorman, Sagar L. Patil et al. "Pan-cancer analysis of lncRNA regulation supports their targeting of cancer genes in each tumor context." *Cell reports* 23, no. 1 (2018): 297-312.

[12] Liang, Wei-Cheng, Wei-Ming Fu, Yu-Bing Wang, Yu-Xin Sun, Liang-Liang Xu, Cheuk-Wa Wong, Kai-Ming Chan, Gang Li, Mary Miu-Yee Waye, and Jin-Fang Zhang. "H19 activates Wnt signaling and promotes osteoblast differentiation by functioning as a competing endogenous RNA." *Scientific reports* 6, no. 1 (2016): 20121.

[13] Yin, Junhao, Xiaoli Zeng, Zexin Ai, Miao Yu, Yang'ou Wu, and Shengjiao Li. "Construction and analysis of a lncRNA-miRNA-mRNA network based on competitive endogenous RNA reveal functional lncRNAs in oral cancer." *BMC medical genomics* 13 (2020): 1-14.

[14] Salimian, Niloufar, Maryam Peymani, Kamran Ghaedi, Sepideh Mirzaei, and Mehrdad Hashemi. "Diagnostic and therapeutic potential of LINC01929 as an oncogenic LncRNA in human cancers." *Pathology-Research and Practice* 244 (2023): 154409.

[15] Norouzinasab, Fatemeh, Niloufar Salimian, Khatere Mokhtari, Mohammadarian Akbari, Mazaher Maghsoudloo, Maliheh Entezari, Afshin Taheriazam, Najma Farahani, and Mehrdad Hashemi. "Discovery of LINC01614 associated with the SPP1 gene in colorectal cancer." *Pathology-Research and Practice* 266 (2025): 155761.

[16] Sayaf, Hossein, Niloufar Salimian, Mahnaz Mohammadi, Parisa Ahmadi, Amir Gholamzad, Sadegh Babashah, Maliheh Entezari, Najma Farahani, Maryam Montazeri, and Mehrdad Hashemi. "Botox-A induced apoptosis and suppressed cell proliferation in fibroblasts pre-treated with breast cancer exosomes." *Molecular and Cellular Probes* 79 (2025): 102007.

[17] Soon, Patsy Siok Hwa, Lyndal J. Tacon, Anthony J. Gill, Christopher P. Bambach, Mark S. Sywak, Peter R. Campbell, Michael W. Yeh et al. "miR-195 and miR-483-5p identified as predictors of poor prognosis in adrenocortical cancer." *Clinical Cancer Research* 15, no. 24 (2009): 7684-7692.

[18] Özata, Deniz M., Stefano Caramuta, David Velazquez-Fernandez, Pinar Akçakaya, Hong Xie, Anders Höög, Jan Zedenius, Martin Bäckdahl, Catharina Larsson, and Weng-Onn Lui. "The role of microRNA deregulation in the pathogenesis of adrenocortical carcinoma." *Endocrine-related cancer* 18, no. 6 (2011): 643-655.

[19] Yuan, Bo, Yasha Liang, Duoning Wang, and Fengming Luo. "MiR-940 inhibits hepatocellular carcinoma growth and correlates with prognosis of hepatocellular carcinoma patients." *Cancer science* 106, no. 7 (2015): 819-824.

[20] Wang, Haiwen, Tao Song, Yanping Qiao, and Jiangtao Sun. "miR-940 inhibits cell proliferation and promotes apoptosis in esophageal squamous cell carcinoma cells and is associated with post-operative prognosis." *Experimental and Therapeutic Medicine* 19, no. 2 (2020): 833-840.

[21] Hou, Lingmi, Maoshan Chen, Hongwei Yang, Tianyong Xing, Jingdong Li, Guangwu Li, Lina Zhang et al. "MiR-940 inhibited cell growth and migration in triple-negative breast cancer." *Medical science monitor: international medical journal of experimental and clinical research* 22 (2016): 3666.

[22] Wei, Jiahui, Yiran Lu, Ruiqing Wang, Xiangzhu Xu, Qing Liu, Song He, Huihao Pan et al. "MicroRNA-375: potential cancer suppressor and therapeutic drug." *Bioscience Reports* 41, no. 9 (2021): BSR20211494.

[23] Lian, Sen, Jung Sun Park, Yong Xia, Thi Thinh Nguyen, Young Eun Joo, Kyung Keun Kim, Hark Kyun Kim, and Young Do Jung. "MicroRNA-375 functions as a tumor-suppressor gene in gastric cancer by targeting recepteur d'origine nantais." *International journal of molecular sciences* 17, no. 10 (2016): 1633.

[24] Jung, Hyun Min, Rushi S. Patel, Brittany L. Phillips, Hai Wang, Donald M. Cohen, William C. Reinhold, Lung-Ji Chang, Li-Jun Yang, and Edward KL Chan. "Tumor suppressor miR-375 regulates MYC expression via repression of CIP2A coding sequence through multiple miRNA–mRNA interactions." *Molecular biology of the cell* 24, no. 11 (2013): 1638-1648.

[25] Chen, Mengjie, Cheng Zou, Yu Tian, Wenchao Li, Yingying Li, and Dingxiao Zhang. "An integrated ceRNA network identifies miR-375 as an upregulated miRNA playing a tumor suppressive role in aggressive prostate cancer." *Oncogene* 43, no. 21 (2024): 1594-1607.

[26] Liang, Xuan, Zhaolun Li, Qunli Men, Yongwei Li, Hechen Li, and Tie Chong. "miR-326 functions as a tumor suppressor in human prostatic carcinoma by targeting Mucin1." *Biomedicine & Pharmacotherapy* 108 (2018): 574-583.

[27] Sun, Chengcao, Chuanfeng Huang, Shujun Li, Cuili Yang, Yongyong Xi, Liang Wang, Feng Zhang, Yunfeng Fu, and Dejia Li. "Hsa-miR-326 targets CCND1 and inhibits non-small cell lung cancer development." *Oncotarget* 7, no. 7 (2016): 8341.

[28] Wu, Lei, Hui Hui, Li-Juan Wang, Hao Wang, Qiu-Fang Liu, and Su-Xia Han. "MicroRNA-326 functions as a tumor suppressor in colorectal cancer by targeting the nin one binding protein." *Oncology reports* 33, no. 5 (2015): 2309-2318.

[29] The Cancer Genome Atlas (TCGA). 2024. "TCGA Program." National Cancer Institute. https://www.cancer.gov/about-nci/organization/ccg/research/structural-genomics/tcga

[30] GTEx 2025 Consortium, Kristin G. Ardlie, David S. Deluca, Ayellet V. Segrè, Timothy J. Sullivan, Taylor R. Young, Ellen T. Gelfand et al. "The Genotype-Tissue Expression (GTEx 2025) pilot analysis: multitissue gene regulation in humans." *Science* 348, no. 6235 (2015): 648-660.

[31] Rishik, Shusruto, Pascal Hirsch, Friederike Grandke, Tobias Fehlmann, and Andreas Keller. "miRNATissueAtlas 2025: an update to the uniformly processed and annotated human and mouse non-coding RNA tissue atlas." *Nucleic Acids Research* 53, no. D1 (2025): D129-D137.

[32] Ritchie, Matthew E., Belinda Phipson, D. I. Wu, Yifang Hu, Charity W. Law, Wei Shi, and Gordon K. Smyth. "limma powers differential expression analyses for RNA-sequencing and microarray studies." *Nucleic acids research* 43, no. 7 (2015): e47-e47.

[33] Ru, Yuanbin, Katerina J. Kechris, Boris Tabakoff, Paula Hoffman, Richard A. Radcliffe, Russell Bowler, Spencer Mahaffey et al. "The multiMiR R package and database: integration of microRNA–target interactions along with their disease and drug associations." *Nucleic acids research* 42, no. 17 (2014): e133-e133.

[34] Huang, Hsi-Yuan, Yang-Chi-Dung Lin, Jing Li, Kai-Yao Huang, Sirjana Shrestha, Hsiao-Chin Hong, Yun Tang et al. "miRTarBase 2020: updates to the experimentally validated microRNA–target interaction database." *Nucleic acids research* 48, no. D1 (2020): D148-D154.

[35] Chen, Yuhao, and Xiaowei Wang. "miRDB: an online database for prediction of functional microRNA targets." *Nucleic acids research* 48, no. D1 (2020): D127-D131.

[36] Li, Jun-Hao, Shun Liu, Hui Zhou, Liang-Hu Qu, and Jian-Hua Yang. "starBase v2. 0: decoding miRNA-ceRNA, miRNA-ncRNA and protein–RNA interaction networks from large-scale CLIP-Seq data." *Nucleic acids research* 42, no. D1 (2014): D92-D97.

[37] Tang, Zefang, Boxi Kang, Chenwei Li, Tianxiang Chen, and Zemin Zhang. "GEPIA2: an enhanced web server for large-scale expression profiling and interactive analysis." *Nucleic acids research* 47, no. W1 (2019): W556-W560.

[38] Vlachos, Ioannis S., Konstantinos Zagganas, Maria D. Paraskevopoulou, Georgios Georgakilas, Dimitra Karagkouni, Thanasis Vergoulis, Theodore Dalamagas, and Artemis G. Hatzigeorgiou. "DIANA-miRPath v3. 0: deciphering microRNA function with experimental support." *Nucleic acids research* 43, no. W1 (2015): W460-W466.

[39] Dennis, Glynn, Brad T. Sherman, Douglas A. Hosack, Jun Yang, Wei Gao, H. Clifford Lane, and Richard A. Lempicki. "DAVID: database for annotation, visualization, and integrated discovery." *Genome biology* 4 (2003): 1-11.

[40] Szklarczyk, Damian, Andrea Franceschini, Stefan Wyder, Kristoffer Forslund, Davide Heller, Jaime Huerta-Cepas, Milan Simonovic et al. "STRING v10: protein–protein interaction networks, integrated over the tree of life." *Nucleic acids research* 43, no. D1 (2015): D447-D452.